PROTEINS: Structure, Function, and Genetics 24:92–114 (1996)

Structure, Energetics, and Dynamics of Lipid–Protein Interactions: A Molecular Dynamics Study of the Gramicidin A Channel in a DMPC Bilayer

Thomas B. Woolf and Benoît Roux
Membrane Transport Research Group (GRTM), Departments of Physics and Chemistry, Université de Montréal, C.P. 6128, Centre-Ville, Canada H3C 3J7

ABSTRACT **The microscopic details of lipid–protein interactions are examined using molecular dynamics simulations of the gramicidin A channel embedded in a fully hydrated dimyristoyl phosphatidylcholine (DMPC) bilayer. A novel construction protocol was used to assemble the initial configurations of the membrane protein complex for the simulations. Three hundreds systems were constructed with different initial lipid placement and conformations. Seven systems were simulated with molecular dynamics. One system was simulated for a total of 600 psec, four were simulated for 300 psec, and two for 100 psec. Analysis of the resulting trajectories shows that the bulk solvent–membrane interface region is much broader than traditionally pictured in simplified continuum theories: its width is almost 15 Å. In addition, lipid–protein interactions are far more varied, both structurally and energetically, than is usually assumed: the total interaction energy between the gramicidin A and the individual lipids varies from 0 to −50 kcal/mol. The deuterium quadrupolar splittings of the lipid acyl chains calculated from the trajectories are in good agreement with experimental data. The lipid chains in direct contact with the GA are ordered but the effect is not uniform due to the irregular surface of the protein. Energy decompositions shows that the most energetically favorable interactions between lipid and protein involve nearly equal contributions from van der Waals and electrostatic interactions. The tryptophans, located near the bulk–membrane interface, appear to be particularly important in mediating both hydrogen bonding interactions with the lipid glycerol backbone and water and also in forming favorable van der Waals contacts with the hydrocarbon chains. In contrast, the interactions of the leucine residues with the lipids, also located near the interface, are dominated by van der Waals interactions with the hydrocarbon lipid chains.** © 1996 Wiley-Liss, Inc.

Key words: phospholipid membranes, permeation, antibiotics, computer simulations, tryptophan, water

INTRODUCTION

In recent years, powerful tools such as X-ray crystallography,[1] electron microscopy,[2] and nuclear magnetic resonance[3] have been developed to characterize the three-dimensional structure of membrane proteins. Despite this progress, many of the factors responsible for the conformational stability of membrane proteins are still not well understood. The difficulties in obtaining detailed information, at the molecular level, about the phospholipid bilayer environment and its influence on lipid–protein interactions contribute to the problem. The dominant effect of the membrane is that of a thermodynamic driving force partitioning the amino acids according to their solubility:[4–6] hydrophobic amino acids are more likely to be found within the hydrocarbon core of the membrane; charged and polar amino acids are more likely to be found in the bulk solvent.[4–6] Much of the complexity of the phospholipid bilayer environment is ignored in such a simplified view. The membrane–solution interface is often pictured as a sharp demarcation between hydrophilic and hydrophobic regions,[7] even though it is likely that the atomic details of the polar headgroup region and the transition from the bulk water to the hydrophobic core of the membrane are important. In fact, the presence of amino acids with aromatic side chains such as tryptophan, tyrosine, and phenylalanine near the interfacial region appears to be a recurrent feature of several membrane proteins, e.g., bacterial photosynthetic reaction center,[1] porins,[8,9] Pf1 and fd viral coat proteins,[3,10] prostaglandin H synthase,[11] the channel formed by the gramicidin A molecule,[12] the peptide segment of hemmagglutinin responsible for influenza virus fusion,[13] and a large series of α-helical human type I membrane proteins.[14] This is supported by results from neutron scattering experiments,[15] showing that the tripeptide Ala-Trp-Ala

Received March 14, 1995; revision accepted July 20, 1995.
Address reprint requests to Benoît Roux, Membrane Transport Research Group (GRTM), Department of Chemistry, Université de Montréal, C.P. 6128, succ. A, Canada H3C 3J7.
Present address of T.B. Woolf: Department of Physiology, John Hopkins University, Baltimore, MD.

has a higher propensity to be located near the interface relative to other residues. An understanding of the factors responsible for the conformational stability of membrane proteins will thus require a better characterization of lipid–protein interactions at the molecular level.

In principle, molecular dynamics simulations of detailed atomic models based on realistic microscopic interactions represent a powerful tool to gain insight into the structure and dynamics of complex macromolecular systems such as membrane proteins.[16] Simulations can provide a wealth of information that is not easily accessible experimentally. In practice, the extension of current computational methodologies to simulate a protein in a fully solvated explicit phospholipid bilayer represents a major challenge. Several detailed studies have reported on the sensitivity of pure lipid bilayer systems to parameterizations of the force field and initial starting conditions (see Pastor[17] for a critical discussion of current problems). For example, fundamental questions have been raised concerning the ability of an empirical potential function based on fixed partial charges with no induced polarization to represent realistically the delicate balance between the hydrophobic and the hydrophilic forces necessary for giving rise to a stable liquid-crystalline bilayer phase.[18] A second difficulty concerns the importance of the starting configuration in pure bilayer systems.[17] The very slow relaxation time scales present in bilayers indicate that several nanoseconds is needed, in principle, for equilibration.[19] This suggests that current trajectories, which are typically on the order of 1 nsec or less, mostly explore the neighborhood of the starting configuration, highlighting the importance of the initial conditions in these simulations. Nevertheless, a number of simulations of bilayers generated with different biomolecular force fields in good qualitative accord with experimental data have now been reported,[20–22] indicating that molecular dynamics of membrane systems are progressing.

Despite the recent success in molecular dynamics simulations of pure phospholipid membranes, similar simulations of a protein embedded in a bilayer have not progressed rapidly. The standard overlay method used for constructing an initial configuration of a protein in bulk solvent, i.e., insertion of the protein structure inside an equilibrated pure water box and deletion of the overlapping waters,[16] does not work in the case of membrane proteins due to the large size of the phospholipid molecules and the significant spatial extent of the lipid acyl chains. In practice, it is almost impossible to create a cavity of the appropriate dimension for inserting a protein by removing a number of phospholipid molecules from an equilibrated bilayer. Thus, an initial starting configuration of a protein embedded in a membrane is difficult to obtain even though configurations of pure phospholipid bilayers are now available from a number of simulations.[20–22]

An alternative to the overlay method is to model build and assemble the bilayer surrounding the protein from its basic components, i.e., the protein, the phospholipid, and the solvent. However, available crystal structures of phospholipid molecules do not provide convenient configurations that can be used as a building block to assemble the protein membrane system.[23] At the temperature of interest, hydrated phospholipid bilayers are in a partly ordered, partly disordered dynamic liquid-crystalline state. The acyl chains of the DMPC crystal are in an all-*trans* conformation, similar to that of the gel state,[24] corresponding to a bilayer thickness of 34 Å whereas X-ray scattering data indicate that the thickness of the hydrocarbon chain region should be about 23 Å for the liquid crystalline L_α state.[25] Furthermore, the crystals contain a very small number of solvent molecules[23] whereas it is known that about 20 waters interact very strongly with the polar headgroups and are needed to recover the solid state NMR spectra of a liquid crystalline bilayer.[26,27] It may be expected that starting configurations constructed from the X-ray structure of phospholipid will be ineffective from a computational point of view because the state of the system differs markedly from those of an equilibrated liquid-crystalline bilayer, e.g., a significant amount of computer time will be required to melt the all-*trans* acyl chains and solvate the polar headgroup properly. Even though the results are independent of the initial state of the system (*in principle*), it is desirable to start the simulation from a configuration that corresponds as closely as possible to the liquid-crystalline state of the bilayer to reduce the computer time needed for equilibration.[17]

To avoid these difficulties, a novel method was introduced for assembling protein membrane complexes from prequilibrated and prehydrated phospholipid molecules.[28–31] The method is an extension of the approach used by Venable et al. to generate pure lipid bilayers.[22,32] The method is general and can be used to construct the initial configuration for membrane proteins of arbitrary shape. In the present study, atomic systems representing the gramicidin A (GA) channel embedded in a fully hydrated dimyristoyl phosphatidylcholine (DMPC) bilayer were generated with this approach. The atomic systems, with a DMPC:GA ratio of 8:1 and 45 wt% water, are models of the oriented samples studied by solid-state NMR in the laboratories of Cross,[12] Cornell,[33] and Davis.[34] The extensively studied GA molecule, which has been used as a prototypical model system both for investigating ion permeation through membranes and lipid–protein interactions, represents an ideal choice for testing the present method. The range of structural, dynamic, and functional data has been summarized

in several recent reviews.[35–37] The influence of GA on lipid motion and order has been characterized through measurements of the deuterium quadrupolar splitting (DQS)[38,39] and FTIR spectra.[40] GA:lipid systems have also been the object of a few theoretical studies based on atomic models. Xing and Scott[41,42] performed Monte Carlo simulations of a the GA channel surrounded by a model bilayer system made of 100 hydrocarbon chains. The simultaions did not include a polar headgroup and the bilayer-like arrangement was artificially maintained by constraining the first carbon of the hydrocarbon chains to move on a plane. Wang and Pullman[43] examined the interactions of GA with glyceryl-monoolate (GMO) molecules disposed in a bilayer-like arrangement. Their study consisted of performing energy minimizations of the GA:GMO system and considered only a single all-*trans* conformation of the lipid molecule. The influence of water, which determines the balance between the hydrophilic and hydrophobic forces in the system, was neglected in both studies. In the present simulations, the solvent (water) is included explicitly and the phospholipid molecules (DMPC) are fully represented with all atoms, including the nonpolar hydrogens. Three hundreds systems were constructed with different initial lipid placement and conformations. Molecular dynamics trajectories were generated for seven systems. One system was simulated for a total of 600 psec, four were simulated for 300 psec, and two for 100 psec. In previous publications,[30,31] the results from the simulation were extensively compared to available structural data from solid-state NMR. The excellent agreement that was observed with available experimental data strongly supports the validity of the current simulations, and suggests that further analysis of the current trajectories can yield much insight about the DMPC:GA system at the atomic level.

In this paper, the structure, energetics, and dynamics of lipid–protein interactions are analyzed in detail. The paper is organized in three sections. The methods for constructing the initial starting configurations, the microscopic model, and the computational details are presented in Methodology. The main results about the average structural properties, water penetration, lipid–protein, and lipid–side chain interactions are discussed in Results and Discussion. Due to its novelty and importance, the method for constructing the initial configurations is also analyzed in this section. A discussion, relating the present study to previous theoretical models addressing the thermodynamics of lipid–protein interactions such as the boundary lipid model of McConnell,[44] the mattress model of Mouritsen and Bloom,[45] and the lattice models of Zuckermann and Pink,[46,47] is also included. The conclusions are then given.

METHODOLOGY

Microscopic Model and Computational Details

The simulation systems represent models for the oriented samples utilized in solid state NMR experiments.[12,33,34] In the experimental systems, the ratio of DMPC:GA is 8:1, and 45 wt% water is used. This corresponds to 16 DMPC molecules, one GA dimer channel, and about 650 water molecules for a total of around 4400 atoms in each microscopic model. The total number of water molecules varied slightly in the different simulation systems due to the method of construction that was used (see below). The three-dimensional structure of the GA channel incorporated in SDS micelles determined by Arseniev et al.[48] using two-dimensional NMR techniques was used as a starting point for the calculations. As in previous work,[49] the initial Arseniev structure was refined with energy minimization using the CHARMM force field and 10 water molecules were included in single-file inside the pore to provide the primary solvation of the dimer. For the simulation systems, the center of the bilayer membrane was located at $Z = 0$, the channel axis was oriented along the Z direction, and hexagonal periodic boundary conditions in the XY direction were applied to simulate an infinite system within the plane of the bilayer (see Fig. 1). Periodic boundary conditions were applied along the Z-direction to simulate a multilayer system. A molecular graphics representation of the system is shown in Figure 2.

The recently developed all-atom PARAM 22 force field of CHARMM,[50] which includes lipid molecules, and the TIP3P water potential,[51] were used for all calculations. The atoms in the DMPC molecules are labeled on the basis of the glycerol moiety as C1 (bound to the headgroup), C2 (bound to acyl chain *Sn*-2), and C3 (bound to acyl chain *Sn*-1). The nonbonded interaction cut-offs followed the work of Pastor et al.[22] on pure lipid bilayers, where the results were excellent. For the trajectories, the nonbonded lists were generated using an atom-based cut-off of 13.0 Å. The electrostatic interactions were smoothly shifted over their entire interaction distance to zero at a cut-off distance of 12.0 Å. The van der Waals interactions were unaffected from 0 to 10 Å and then switched from 10.0 to 12.0 Å to zero. Automatic update of the nonbonded list was used for the nonimage interactions. An update frequency of every 5 steps was used for the nonbonded interactions involving the image atoms. This update frequency for the image atoms was chosen to maximize the efficiency of the automatic nonbonded list update, by not regenerating the nonbonded list involving image atoms too frequently.

The trajectories were calculated in the microcanonical ensemble with constant energy and volume. Different cross-sectional areas were chosen in the XY plane. The majority of the simulation time was

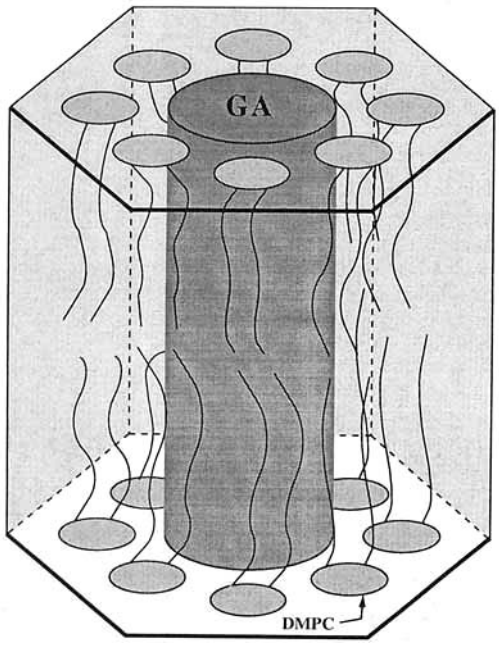

Fig. 1. Schematic three-dimensional view of the simulation system (not drawn to scale). Periodic boundary conditions using hexagonal symmetry are applied in the *X* and *Y* directions, translational symmetry is applied along *Z* (the simulation system is effectively a DMPC:GA multibilayer). The central part of the cell contains the gramicidin (GA) channel surrounded on each side by eight DMPC lipid molecules.

devoted to study systems with a cross-sectional area of 764 Å^2. This corresponds to an edge length for the hexagons of 17.2 Å. A *Z*-translational distance of around 60 Å was used, with slight variations depending on the initial water structure after construction (see below). The average temperature was 340 K, above the gel-liquid crystal phase transition, and consistent with experimental conditions.[52] The length of all bonds involving hydrogen atoms was kept fixed with the SHAKE algorithm.[53] The equations of motion were integrated with a time-step of 2 fsec. Equilibration dynamics consisted of three different stages. In the initial stages, Langevin dynamics was used to apply a uniform temperature of 340 K throughout the system, the GA channel backbone was fixed, and planar harmonic restraints with a force constant of 0.5 kcal/mol-Å^2 were applied to the DMPC phosphate atoms that deviated by more than 1.5 Å from reference *Z*-values of ±18 Å. The harmonic restraints were gradually decreased, so that by the end of 50 psec, the GA channel and the full system were completely free. In the following 25 psec, the velocities were scaled every 0.5 psec to adjust the temperature. No velocity scaling was applied during the last 25 psec of equilibration and the temperature remained stable.

Seven different systems were selected for detailed simulation from the ensemble of 300 generated during the construction process (see below). The final trajectory from one of these systems was of 600 psec in length. Four systems were simulated for 300 psec. Two other systems, using smaller and larger cross-sectional areas in the *XY* plane, were simulated for 100 psec each. For each system, extensive analysis of average structural and dynamic properties was performed.

Construction of Starting Configuration

A specially designed method was used for generating the starting configurations used for the DMPC:GA simulations. The starting configurations were assembled from preequilibrated and prehydrated DMPC molecules in order to be as closely in accord as possible with all available experimental data about DMPC and GA. This novel method was used to avoid the long simulation times that would otherwise be needed to equilibrate the system. The preequilibrated conformers for each DMPC molecule were taken randomly from a set of 2000 that was previously generated from Monte Carlo simulation of an isolated DPPC molecule in the presence of a mean field.[19,22,32] Each conformer was prehydrated by constructing approximately 20 water molecules around the phosphate and choline groups based on the results of previous molecular dynamics simulations of isolated PC headgroups.[54] The parameters of the mean-field were empirically adjusted to reproduce such experimental observables as the ^{2}H quadrupolar splitting order parameters and the ^{13}C NMR relaxation times.[19,55,56] The conformers generated by the mean-field Monte Carlo simulations, in so far as they agree with the available experimental data, are representative of the phospholipid molecules found in a bilayer membrane in thermal equilibrium with its normal axis in the *Z* direction. To provide the primary hydration for the polar headgroup, 20 water molecules were constructed around both the phosphate and the choline group of all the lipid conformations. The primary waters were constructed in accord with their calculated spatial distribution based on molecular dynamics simulation of *o*-phosphorylcholine (*o*-PC) in bulk solution.[54] The 20 primary waters provide approximately 80% of the total solvation energy of *o*-PC in bulk solution.[54] A typical sample of 16 DMPC molecules chosen randomly from the library is shown in Figure 3 (those are the lipid conformers used to construct the initial configuration used in the simulation of 600 psec).

Optimal lateral packing of the hydrocarbon chains of the lipids in the plane of each leaflet of the bilayer is important for the starting configuration. However, such packing is difficult to achieve using random placements of lipids around the GA as was done to construct pure lipid bilayers.[22,32] The general strategy for creating a reasonable starting point for the DMPC within the 8:1 DMPC:GA system was to randomly select 16 lipids from the preequilibrated

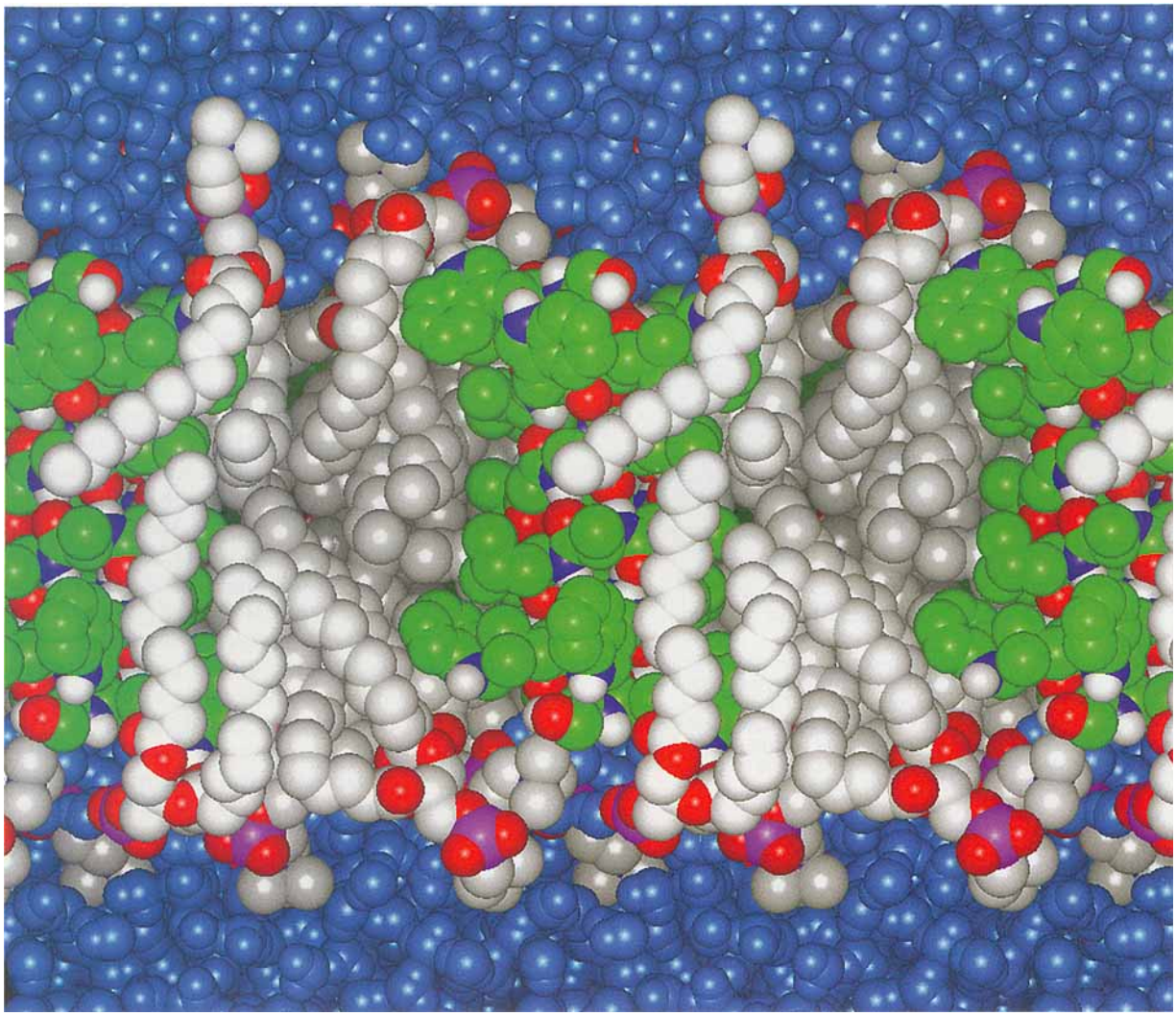

Fig. 2. Molecular graphics representation of one configuration of the periodic 8:1 DMPC:GA system. The color coding is: oxygen (red), nitrogen (blue), phosphorus (magenta), protein hydrogen (white), protein carbon (green), lipid carbon (gray) and water (aqua marine blue). Lipid hydrogens are not shown for the sake of clarity. Some image atoms from the periodic boundary conditions are shown (e.g., the GA channels on the left and right). There are 4387 atoms in the central system. The snapshot was taken after 550 psec from a trajectory of 600 psec (see text for details).

and prehydrated set, place them around the GA, and then reduce the number of core–core overlaps between heavy atoms through systematic rotations (around the Z-axis) and translations (in the XY plane) of the DMPC and the GA. To provide the initial XY positions for each lipid, the full DMPC molecule was represented by a single effective particle corresponding to its average cross-sectional area. The effective lipid particles were modeled as large Lennard–Jones spheres of 4.8 Å radius. The packing of the effective lipid particles around the protein was determined from a molecular dynamics simulation in which the large Lennard–Jones spheres were constrained along Z and freely moving in XY with the hexagonal periodic boundary conditions. Because the GA dimer is not sufficiently long and does not overlap with the average position of the phosphate groups, the coordinates of each GA monomer were projected onto a single Z plane ($\pm$18 Å) and eight Lennard–Jones spheres were uniformly placed around each of the flattened monomers. The large spheres representing the effective lipids were free to move within the XY plane at $Z = \pm 18$ Å. More generally, no such projection of the coordinates would be needed in the case of large intrinsic membrane proteins, protruding well outside the bilayer, and a direct simulation of the Lennard–Jones spheres restrained to the planes corresponding to the headgroup region could be performed. After energy minimization and dynamics, the resulting XYZ

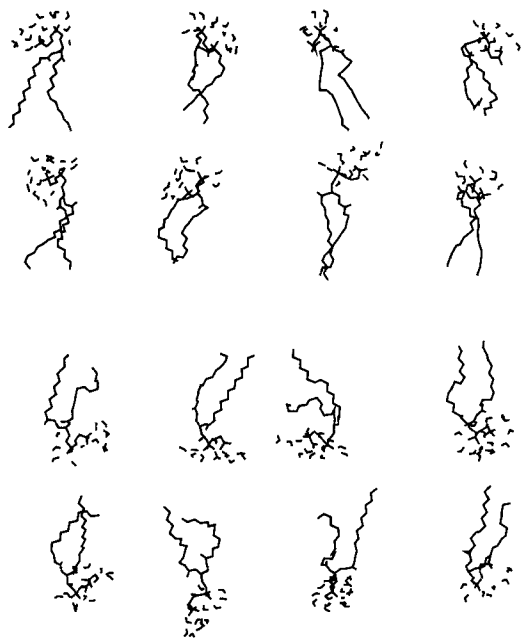

Fig. 3. Typical sample of 16 preequilibrated and prehydrated DMPC molecules chosen randomly from the library of 2000.

positions of the large spheres were utilized for the initial *XYZ* placement of the phosphate of each DMPC. The chosen construction corresponds to a membrane thickness of 36 Å to accommodate the slight thickening predicted experimentally for the GA:DMPC systems relative to a pure DMPC bilayer.[25,39]

Because the initial systems are assembled with uncorrelated phospholipid conformers, the number of bad contacts is considerable. To improve the initial structure and decrease the number of bad contacts while still maintaining the conformation of the preequilibrated and prehydrated DMPC lipids, an optimization based on a global search, using systematic rigid body rotations and translations of the lipids (with their primary waters) and the central GA, was performed. The search for the optimized initial configuration for a particular set of lipids around the GA was aimed at minimizing the number of bad contacts (defined as a distance of less than 2.6 Å between heavy atoms of the system). Systematic rotations were performed consisting of rigid body rotations around the *Z*-axis in 10° increments for each individual lipid followed by a similar series of rotations for the GA. Systematic translations in the *XY* plane were performed consisting of 0.25 Å steps around a square of side 2 Å centered on the initial placement of each lipid. This method decreased by a factor of two or more the number of bad contacts within each system. Three sets of 100 systems, corresponding to different *XY* cross-sectional area, were generated using this construction method. Using the described procedure, only a small fraction of the configurations generated were found to have hydrogen bonding involving the N-H group of the tryptophan indole ring. Based on hydrogen exchange[57] and IR and Rahman spectroscopy experiments,[58] it is believed that two of the four tryptophans are hydrogen bonded with water, one is bonded moderately and one is bonded weakly if at all. A reasonable interpretation of these results is that Trp-13 and Trp-15 are often involved in hydrogen bonding, Trp-11 is sometimes involved, and Trp-9 is not. To increase the number of systems having hydrogen-bonding patterns in accord with the experimental results, a biasing weighting function was introduced for the initial optimization of the system. A negative weight equivalent to a decrease of 10 in the total number of bad contacts was awarded for each Trp-13 or Trp-15 indole N-H in hydrogen-bonded contact with either a water or DMPC carbonyl group. No shift in the total bad contacts was based on the hydrogen bonding pattern of Trp-11. An increase of 10 in the total number of bad contacts was introduced for hydrogen bonds with Trp-9. The procedure increased the number of generated configurations with hydrogen bonding in accord with the experimental information, even though the total number of bad contacts did not increase markedly relative to systems constructed without this penalty. Ultimately, the analysis of the trajectories indicated that this procedure was not necessary and that rapid fluctuations of the hydrogen bonds involving the indole N-H were observed (see below).

After the global search based on systematic rotations and translations, the remaining unrealistic bad contacts between heavy atoms of the system were removed by using several cycles of energy minimization. The ABNR algorithm was used for all the minimization.[59] For each cycle, the Lennard–Jones radii of the heavy atoms were gradually increased. The GA channel remained fixed. This procedure gradually removed the remaining bad contacts without perturbing the overall lipid conformers. On average, the energy minimization cycle resulted in atomic displacements on the order of 0.8 Å relative to the initial system.

To obtain a microscopic system with 45 wt% water, the remaining bulk solvent was constructed using a slab of 738 waters equilibrated using the same *XY* hexagonal periodic boundary conditions. The water box was translated along the *Z*-axis and its position was adjusted to give the correct total number of waters for the system. All waters that projected into the hydrocarbon interior of the bilayer, between ±14 Å in the *Z* direction, were deleted. After the overlay, energy minimization was performed for 200 steps using the steepest descent algorithm before dynamics was initiated.

TABLE I. DMPC Cross Sectional Area

Area Å^2	Reference	Method
56	Pace and Chan, 1982[62]	NMR
57.6–70.9	Nagle and Wiener, 1988[63]	X-ray
58.6	Schindler and Seelig, 1975[64]	NMR
62 ± 2	Nagle, 1993[65]	NMR
65.7	Lewis and Engelman, 1982[25]	X-ray
69	DeYoung and Dill, 1988[66]	NMR
71.7	Thurmond et al., 1991[67]	NMR
68.9	Pastor et al., 1991[32]	MD

RESULTS AND DISCUSSION

Choice of System Size and Initial Construction

The choice of cross-sectional area for the hexagonal simulation system must be carefully determined because it has an important influence on the state of the bilayer system. Prior modeling studies of pure bilayer systems illustrate the importance of the cross-sectional area.[60] An underestimated cross-sectional area may shift the system from a liquid-crystalline state to a more gel-like state,[60] whereas an overestimate can lead to an unstable disordered bilayer. Neither of these extremes would correctly model the lipid–protein interactions in a liquid-crystalline membrane. The present simulations were carried out at constant volume simulation, and the cross-sectional sets the lateral pressure on the GA and the lipid. The possibility of using a constant pressure algorithm will be considered for the future, but difficulties remain in applying current methodologies to molecular systems involving long connected molecules with significant amounts of anisotropy in the X, Y, and Z directions.[61] Moreover, even with constant pressure methods it is necessary to construct the initial configuration using a reasonable value of the cross-sectional area.

The cross-sectional area of DPPC has been investigated more extensively than that of any other lipid molecule using a variety of experimental methods. Despite this amount of work, the size of the average cross-sectional area for DPPC in the L_α phase is still not known with great confidence. Table I shows the range of experimental and calculated results for the DPPC lipid molecule. Using NMR estimates from the order parameters, experimental estimates ranging from 52 to 74 Å^2 have been published. Using either X-ray diffraction or pressure/area measurements performed with Langmuir monolayers spread at the air–water interface, a similar range of cross-sectional areas has been published. There are also estimates available from molecular dynamics calculations, with 68.9 Å^2 being the most recent estimate.[32] Thus, an estimate for the DMPC cross-sectional area, which is assumed to be in the same range as the DPPC area, is around 62 Å^2 but it could vary from 52 to 74 Å^2.

Estimates for the cross-sectional area of GA are more uncertain than for lipid molecules. Table II shows the range of experimental and calculated estimates for the GA cross-sectional area. The experimental values range from 110 to 305 Å^2, with the most frequently used estimate being 250 Å^2. The experimental estimates were mainly obtained using the Langmuir trough method. This method is based on measurements of the area of lipid monolayers spread at an air–water interface as a function of applied lateral pressure. The range of experimental numbers reflects the difficulty in interpreting the transitional points in pressure/area measurements.[67–72] For example, phase transitions from different packing arrangements and/or conformational changes can occur at various points along the pressure/area curves. The early estimates suggested about 150 Å^2 for the GA channel.[67] Later work suggested that this area corresponded to the double-helix form of the GA and that another transition in the pressure/area curve was identified with the head-to-head channel conformation.[70] The significance of the results is somewhat limited. For instance, it is not certain that measurements obtained from monolayers can be extended to provide a valid representation of the bilayer environment. Furthermore, it remains unclear whether the GA adopts the β-helical head-to-head channel conformation in a Langmuir monolayer spread at the air–water interface and if the features of the pressure/area curve are due to changes in conformation, orientation, or packing motif during the measurements.[70,72] Despite those limitations, Table II summarizes all presently available estimates of cross-sectional area.

Calculated estimates of the cross-sectional area for the GA channel from models of the channel conformation depend on the area of the probe used to determine the molecular surface. If the lipids are pictured as undeformable rigid objects with an effective radius of 4.8 Å, a cross-sectional area of 528 Å^2 is obtained. In contrast, if the hydrocarbon chain region is pictured as a liquid-like collection of free methylene atoms with an effective rigid radius of 2.2 Å, a cross-sectional area of 328 Å^2 is found. These estimates are reduced to 405 and 228 Å^2 if the cross section is calculated by including only the backbone atom and the carbon C_β. To find a cross-sectional area of 250 Å^2 corresponding to the experimental estimate, a probe radius of 1.3 Å should be used (2.6 Å if only the backbone with C_β atoms are included). These numbers are also listed in Table II for comparison with the experimentally determined numbers. It is intriguing that such a small probe radius (the radius of a methylene atom is 2.2 Å) is necessary for agreement with the experimental number. This suggests that the local packing of the hydrocarbon chains around the GA should be viewed as more similar to that of free methylene groups rather than rigid DMPC molecules.

The experimental estimates for DMPC and GA,

TABLE II. Gramicidin Cross-Sectional Area

Area Å^2	Reference	Method
110–160	Ries and Swift (1987)[70]	Air/water
145 ± 10	Kemp et al. (1972)[68]	Air/water
150	Haydon and Hladkey (1972)[82]	Model building
200	Kemp and Wenner (1976)[69]	PC-monolayer
215	Urry et al. (1971)[83]	Model building pi(6-L,D)
225	Tournois et al. (1989)[73]	Air/water
235–305	Dhathathreyan et al. (1988)[71]	Air/water w/FTIR
250 ± 25	Mau et al. (1987)[72]	Air/water
250	He et al. (1993)[89]	X-ray (assuming DLPC of 52 Å^2)
405*	This work	Calculated with probe radius of 4.8 Å
228*	This work	Calculated with probe radius of 2.2 Å
250*	This work	Calculated with probe radius of 2.6 Å
528†	This work	Calculated with probe radius of 4.8 Å
328†	This work	Calculated with probe radius of 2.2 Å
250†	This work	Calculated with probe radius of 1.3 Å

*Calculated with backbone and C_β atoms only of the GA.
†Calculated with all atoms of the GA.

give bounds to the cross-sectional area of the entire 8:1 DMPC:GA system through the relation:

$$A_{tot} = 8 \times A_{DMPC} + A_{GA} \quad (1)$$

The result is a set of possible system sizes ranging from 526 to 897 Å^2. The cross-sectional area of the system corresponds to a center-to-center distance between neighboring hexagonal cells through the relation $h = 2 \times \sqrt{A_{tot} \cos^2(\pi/6)/3}$, where h is the center-to-center translational distance from one hexagon to another and A_{tot} is the total system cross-sectional area. Thus the smallest and largest possible system sizes correspond to translational distances of 24. and 32.2 Å. The three systems sizes that were considered used translational distances of 27.7, 29.7, and 32.0 Å, which correspond to system sizes of 664, 764, and 887 Å^2, respectively.

Figure 4 shows the change in the number of bad contacts for the 300 configurations generated with the three different total cross-sectional areas. As expected, the more compact system has the highest initial number of bad contacts. This is easily understood by the more confined packing arrangement in a denser system. The other two sets of systems have nearly half as many bad contacts in the initial construction. The variation in the number of bad contacts within one set of 100 conformations reflects the degree of initial fit between the randomly chosen lipids and the GA structure. Following the initial construction, systematic rotations and translations of the hydrated DMPC decreased considerably the number of bad contacts. This is also shown in Figure 4. The degree of change did vary somewhat between the three different XY cross-sectional areas used, but generally the number of bad contacts between the initial randomly packed systems and the optimized systems with systematic rotations and translations decreased by a factor of two.

It was observed that the resulting state of the protein membrane complex was quite sensitive to

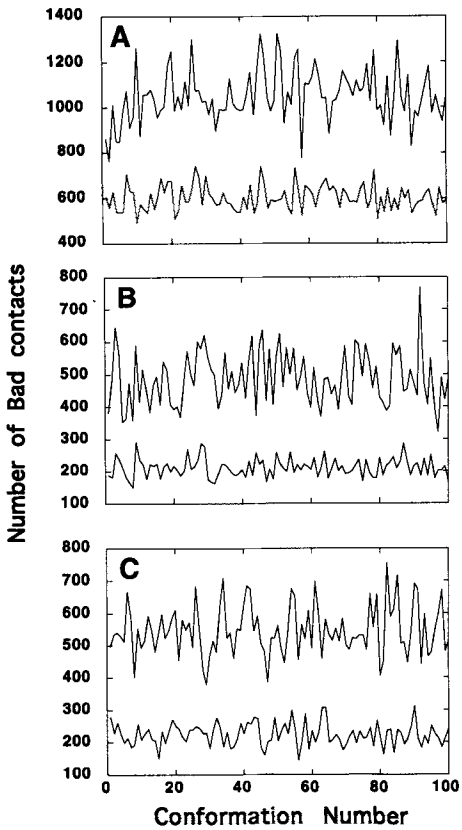

Fig. 4. Number of bad contacts for three different choices of system size. The total cross-sectional area was 664 (**A**), 887 (**B**), and 764 Å^2 (**C**). **A** and **B** are for systems constructed without a penalty function to influence the number of hydrogen bonds, whereas the systems **C** were constructed with a penalty function. In each case, the systematic rotations and translations reduced the total number of bad contacts by more than a factor of two. The more compact system (**A**) had a significantly higher number of bad contacts. The penalty function used for the systems of **C** did not significantly change the total number of bad contacts in the system (data not shown).

the cross-sectional area of the simulation system. The three different sizes used for constructing DMPC:GA systems led after equilibration to differences in the phosphate-to-phosphate distance and the ratio of *trans/gauche* conformers in the hydrocarbon chains. The smallest cross-sectional area of 664 Å^2 led to a decrease in the number of *gauche* conformations for the hydrocarbon chains from 35 to 25%, and to an increase in the bilayer thickness from 36 to 40 Å over the trajectory. The largest system size of 887 Å^2 led to large movements of the hydrocarbon chains, approximately 10% increase in the number of *gauche* bonds and frequent water penetration in the hydrocarbon region. An intermediate system size of 764 Å^2, corresponding to a cross-sectional area of 250 Å^2 for the GA and 62 Å^2 for the 8 DMPC molecules, led to a stable bilayer thickness and an overall slight increase in the number of *trans* conformations and no frequent water penetration in the hydrocarbon region. Previous analysis of the 600 psec trajectory generated with a cross-sectional area of 764 Å^2 indicated that calculated solid-state NMR properties, such as the ^{15}N chemical shift, the N-H dipolar coupling, and the $^2H_\alpha$–C_α deuterium quadrupolar splittings of the backbone were in excellent accord with experimental data.[30,31] For these reasons, the 664 and 887 Å^2 systems were not considered further in the following analysis.

To examine the variations in the intramolecular conformations of the protein and the lipid within the complex bilayer environment, the root-mean-squared (rms) difference with respect to a reference structure was calculated. The rms variations in the GA and the lipid with respect to their initial structures (at t = 0) are presented in Figure 5 for the 600 psec simulation. The time from −100 to 0 psec corresponds to the equilibration period. The rms difference for the DMPC was averaged over the 16 molecules in the system. From −100 to −50 psec of the simulation, the rms deviation of the GA structure is less than 0.5 Å because the backbone was fixed and only the side chains were allowed to move. The structural fluctuations reached a plateau within 150 psec, with an rms difference from the Arseniev structure of about 1.2 Å. The relative magnitude of the fluctuations was also conserved with the other four systems, where the rms deviations were on the order of 1.8, 1.6, 1.2, and 1.2 Å (data not shown for the sake of clarity). The backbone of GA showed a relatively small variation throughout all five systems. Further analysis of the trajectories showed that most of the nonpolar residues with aliphatic side chains did undergo isomerization transitions between multiple conformations whereas the Trp side chains were fluctuating around unique conformations with the N–H group indole pointing toward the bulk solution. The calculated ^{15}N chemical shift, N–H dipolar coupling and the deuterium quadrupolar splittings of the Trp indole ring were in excellent

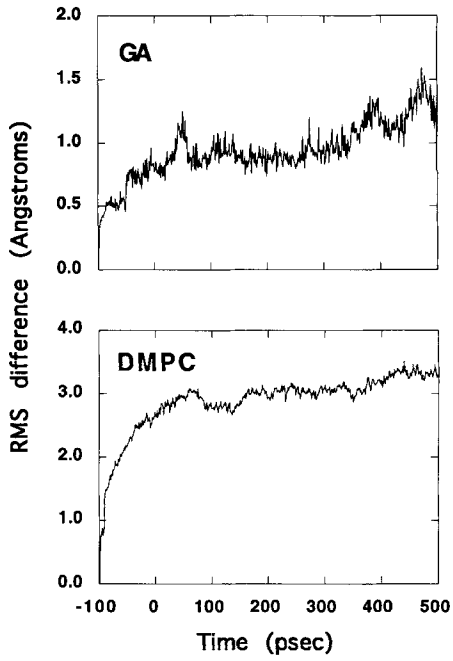

Fig. 5. Rms differences during the full simulation for GA and lipids relative to the initial structure taken at time t = −100 psec. The left-hand column presents the difference between the Arseniev structure and the simulated GA. The right-hand column shows the difference from the initial lipid structures averaged over all 16 lipids. Similar rms differences were seen for the other four systems.

agreement with available solid-state NMR data, indicating that the orientation of the Trp side chains at the membrane–solution interface is essentially correct.[30,31] In contrast, the rms differences between the lipids and their initial starting structure were larger and reached a plateau at about 3.0 Å. A similar magnitude was observed for the other four systems (on the order of 3.0, 3.5, 3.0, and 3.5 Å). The changes in the lipid conformation are more pronounced along the acyl chains and more modest in the polar head and glycerol region. Figure 6 shows the fraction of *gauche* conformations in the acyl chains averaged over both chains and all dihedrals as a function of simulation time. During the equilibration period (from −100 to 0 psec), there is a slight decrease of the fraction of *gauche* conformations corresponding to an ordering of the acyl chains. Similar ordering of the lipid chains in direct contact with the GA was also observed in the Monte Carlo simulations performed by Xing and Scott.[41,42] A closer examination shows that the *gauche*$^+$ and *gauche*$^-$ were both equally populated (around 12–15% each).

The existence of a plateau in the fraction of *gauche* conformations beyond the initial variation shown in Figure 6 suggests that a period of 100 psec was adequate to equilibrate the systems constructed with the present protocol. However, because MD simulations remain relatively short on the time

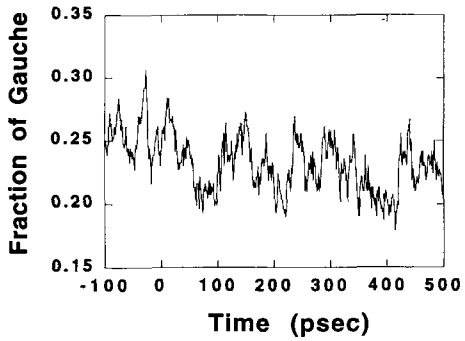

Fig. 6. Total fraction of *gauche* dihedral angles as a function of time for both chains throughout the equilibration period (from −100 to 0 psec) and the production trajectory (from 0 to 500 psec).

scale of bilayer dynamics[17,19] it is of interest to examine the extent of the configurational sampling reached in the present calculations. The maximum rms deviation of a DMPC molecule is expected to be on the order of 4.0 Å based on an estimate between a random subset of 1000 pairs taken from the 2000 member preequilibrated DMPC library. This number is slightly larger than the plateau value reached in the five simulations. This indicates that a large amount of the fluctuations of the phospholipid is sampled effectively on the relatively short time scale (on the order of 100–200 psec). It can be expected that the equilibration time would have been much longer if the simulation had started from an all-*trans* acyl chain conformation. The fact that the rms fluctuations of the DMPC molecules reached a plateau at 3.0 Å within 300 psec for all five simulated systems suggests that doubling the length of the four shorter trajectories would not have produced any new results and that significantly longer trajectories (on the order of 2–3 nsec) could be necessary to reach extensive conformational sampling in the system.[19] The need for a very long trajectory is somewhat reduced by the present approach because configurational averaging can be obtained from an *ensemble* of independent simulations. In the following analysis, all averages were obtained from configurations taken after the initial equilibration period of 100 psec.

Average Structural Properties

The average distribution of various components along the bilayer normal provides information on the organization of the membrane–protein system. Figure 7 shows the average density profile for the main components of the DMPC:GA system calculated from the 600 psec simulation (the profiles calculated from the four 300 psec simulations are similar and are not shown for clarity). The resulting profiles are similar to those that are measured by X-ray[25] and by neutron scattering of oriented multibilayer systems.[73,74] In the top part of the figure, the average density for the water, the hydrocarbon chains, the ester oxygens of the glycerol region of the DMPC lipids, the phosphate and the nitrogen of the PC headgroup, and the heavy atoms of the GA backbone are shown. Several important features provide a complete picture of the average organization of the main components of the DMPC:GA system. The backbone atoms of the GA system occupy the region within 24 Å on both sides of the bilayer center. The average probability of the hydrocarbon chains is reduced near the center of the bilayer system, in accord with both experiment and other molecular dynamics simulations.[21,22,74] The bulk water probability falls from the region outside the channel to a single file of hydrogen-bonded waters inside the GA channel. The water density profile makes a transition from about 20 Å to about 10 Å, with a small plateau around 15 Å due to the lipid headgroups. The headgroup and glycerol regions span a region of 15 Å in width, with the carbonyl oxygens of the ester group of the lipids being found on average from about 10 to 20 Å. The P and N atoms of the headgroup are generally located within the same region along Z but the density for the N atoms is slightly more spread out than that for the P atoms. This reflects the fact that the headgroup dipoles are aligned parallel to the membrane plane on average. The observed orientation of the headgroup is in general accord with ^{31}P solid-state NMR chemical shifts measurements of pure bilayers.[75,76] The ^{31}P chemical shifts anisotropy was calculated to be −33 ppm for the 600 psec trajectory,[31] in excellent agreement with the experimental value of −34 ppm.[77] Nevertheless, considerable fluctuations about the average orientation are present. The P–N vector can fluctuate within a window of plus and minus 50° from the plane of the bilayer. The importance of the observed fluctuations in the orientation of the polar headgroup suggests that the experimental data are better interpreted in terms of an average over an ensemble of configurations.[31,78]

Further details of the bilayer system, can be seen in the lower part of Figure 7, where a region from 5 to 20 Å of the density profiles in the top part is magnified to show the transition from the single-file water region to the bulk water region. The density profile of the N–H group of the indole rings is shown for each of the four tryptophans of the GA system. It is particularly interesting that the distribution of the carbonyl oxygens of the ester group of the DMPC lipids is peaked in the same region, though it overlaps more with Trp-13 and Trp-15 relative to Trp-11 and Trp-9. This observation suggests that hydrogen bonds between the lipid ester carbonyl groups and the hydrogens of the trytophan rings of the GA channel are structurally possible. This point is discussed further below.

Whereas the density profile provides information about the average organization of the DMPC:GA

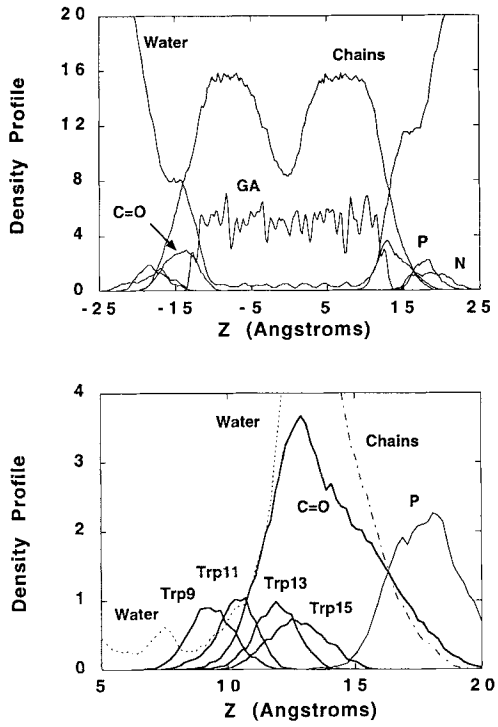

Fig. 7. Average density profile of various components in the simulation systems. The profile was computed as a time average over all conformations from the 600 psec trajectory after the 100 psec equilibration period. A bin size of 0.2 Å was used. The normalization is arbitrary.

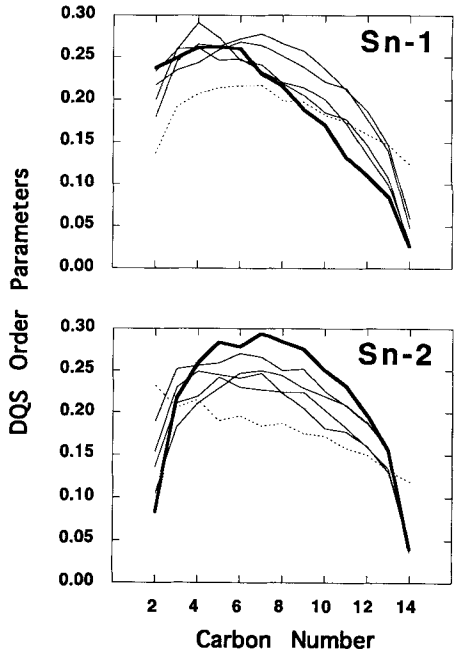

Fig. 8. Deuterium quadrupolar splitting (DQS) order parameters calculated on the basis of Eg. (2) for the five simulations. The results for the chain 1 and 2 of DMPC are shown. Rms fluctuations on the order of 0.1 were observed for the average from a given trajectory.

system, it does not reveal the intramolecular conformation of the lipid acyl chains. Acyl chain order parameters extracted from deuterium quadrupolar splittings (DQS) have been used to characterize the motion and acyl chain order of the phospholipid in contact with the channel.[38] The DQS order parameter at the ith carbon position, $S_{CD}^{(i)}$, is calculated from a time-average,[38]

$$S_{CD}^{(i)} = \left\langle \frac{3\cos^2[\theta^{(i)}{}_{(t)}] - 1}{2} \right\rangle \qquad (2)$$

where $\theta^{(i)}{}_{(t)}$ represents the instantaneous angle between the director of the $C^{(i)}$–D bond and the axis of rapid reorientation (here the bilayer normal directed along the Z-axis). The DQS order parameters calculated from the five different simulations are shown in Figure 8. Although there are significant variations, the trends from the different simulated systems are similar. All simulated systems exhibit a higher acyl chain order relative to the library of pure DMPC (indicated with a dashed line) and the shape of the order profile is similar with a maximum near carbon 3–4 in chain *Sn*-1 and near carbon 6–7 in chain *Sn*-2. The rms fluctuations in the order parameter of individual carbon was on the order of 0.1 to 0.3. Due to the long time scales involved in the relaxation of the hydrocarbon chains and the limited configurational sampling, the statistical uncertainty of the calculated DQS from each trajectory is significant. To obtain a better estimate of the DQS in the DMPC:GA system, an *ensemble* average can be performed. The results from the five independent trajectories were combined according to a weighted average proportional to their simulation length (excluding the equilibration period, i.e., 500, 200, 200, 200, and 200 psec). In Figure 9, the results for chain *Sn*-2 are compared with the experimental data obtained by Rice and Oldfield in 1979 from specifically labeled DMPC at a 15:1 molar ratio.[38] Despite the slight differences in external conditions (temperature and GA concentration), the calculated DQS order parameters are in remarkable agreement with the experimental data. In particular, carbons 6 and 7 exhibit the largest ordering relative to pure DMPC. Further analysis indicated that the DMPC acyl chains have an increase in *gauche* conformers at the first and last bonds relative to a pure DMPC bilayer. FTIR data for a DPPC:GA system at 10:1 molar ratio also indicate that there is an increase of *trans* conformer at carbon position 10.[40]

Because the DQS of the lipid acyl chains have a complex dependence on the concentration of GA, the interpretation of experimental data has been the object of some controversy over the years. Experimentally, it is observed that the DQS increase linearly

with GA concentration. A maximum value is reached at a DMPC:GA molar ratio of 15:1 where the DQS are 30% greater than those of pure DMPC. For higher concentration, the DQS decrease until an abrupt variation in the DQS occurs at a molar ratio of 4:1, indicating the presence of important structural transformations in the bilayer system.[38] Rice and Oldfield suggested that the irregular surface of the GA induces a disorder along the acyl chains of the lipids in direct contact with the channel whereas the boundary lipids surrounding the GA present a smoother surface, which, in turn, orders the next layer of lipids.[38] According to this interpretation, the observed variations in DQS as a function of GA concentration result from the change in the population of boundary lipids versus free lipids. An alternative explanation was provided by Pink et al.[79] within the context of a theoretical model. It was argued that the lipids in direct contact with one GA channel are ordered, whereas the lipids in contact with two or more GA at higher concentration are disordered. The present results, corresponding to a 8:1 molar ratio, indicate that there is an ordering of the lipid chains in direct contact with the GA channel. However, due to the irregular surface of the GA the lipid chains are not ordered uniformly. The first and last carbons along chain *Sn*-2 are almost unchanged relative to pure DMPC. In contrast, carbons 6 and 7 of chain *Sn*-2 exhibit the highest ordering. Those carbons are typically located between 8 and 10 Å from the center of the bilayer. A majority of the closest contact of carbon 6 and 7 of the *Sn*-2 chain with the channel are with the tryptophan side chains (75%). More particularly, the outer atoms of the indole ring $C_{\zeta 2}$, $C_{\eta 2}$, $C_{\zeta 3}$, and $C_{\epsilon 3}$ are the closest to the lipids. A particular packing arrangement of the hydrocarbon chains in direct contact with the channel can be seen in the snapshot shown in Figure 2 (see also the analysis of hydrogen bonds involving the tryptophan indole rings, below). The chains are most ordered for carbon 4–7 due to the packing along the surface of the tryptophan side chains. The end of the chains (carbon 10–14) reaches under the bulky tryptophan side chains and is not ordered by the channel. The ordering of the chains results in a slightly increased thickness of the bilayer.[80] In all five simulations, the bilayer thickness determined as the phosphate-to-phosphate distance was slightly larger than expected for a pure DMPC bilayer: the value remained stable at 36 Å, in contrast to the value of 34 Å expected for a pure DMPC bilayer.[25] Although it is possible that the thickening of the bilayer is related to the fixed cross-sectional area of the simulation system in the present simulations, it is consistent with the ordering of the DMPC molecules.

Water Penetration

Penetration of water molecules into the hydrophobic core of the bilayer is an important indication

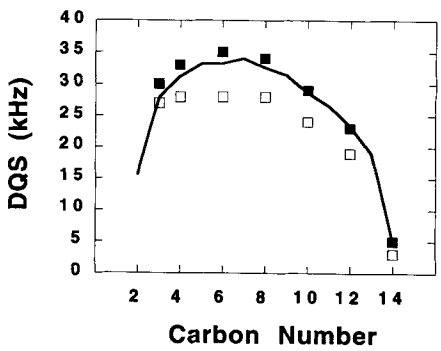

Fig. 9. Deuterium quadrupolar splitting (DQS) of the chain *Sn*-2 of DMPC. The results were obtained as a weighted average over the five trajectories shown in Figure 8. The experimental data for pure DMPC (empty squares) and for a 15:1 DMPC:GA observed at 30°C (filled squares) are also shown.[38] The frequency splittings, which were measured from a multilamelar dispersion, are related to the order parameter by (3/4) 180 kHz $|S_{CD}^{(i)}|$.[38]

of the thermodynamic stability of the simulation system. As mentioned above, a large number of water molecules were observed in the simulation with an overestimated cross-sectional area (887 Å^2). In the 764 Å^2 system, a small number of excursions by water molecules inside the hydrocarbon region of the bilayer were observed, although the average structure of the membrane–protein complex remained stable throughout the five simulations. Figure 10 shows the time series of those waters that penetrated the lipid bilayer during the longest trajectory. Three water molecules (84, 484, 633) entered the exited the bilayer region within 5 psec. One water molecule (386) entered the bilayer and formed a stable hydrogen bond to the backbone outside the channel. The event consisted of two stages. In the first stage (at 400 psec), the water (386) entered and was not stably bound. In the second stage (at 490 psec), the water moved further into the bilayer and formed a stable hydrogen bond to the outer surface of the channel with the amino hydrogen of Leu-4 and with the carbonyl oxygen of Trp-9. The interaction energy between the GA and the outside-bound water was on the order of −9 kcal/mol. Thus, the presence of the protein appears to be directly responsible for the stabilization of this water molecule inside the bilayer. Interestingly, it has been shown using fluorescence lifetime measurements that gramicidin is responsible for increasing the presence of water molecules in the hydrocarbon region of 1-palmitoyl-2-oleoyl-phosphatidylcholine (POPC) bilayers.[81] More generally, increase in water penetration inside bilayers has also been observed in neutron scattering experiments in the presence of small peptides.[15]

Despite the fact that they are involved in hydrogen bonding in the β-helical GA dimer, the carbonyl groups of the backbone remain accessible for forming hydrogen bonds with water molecules entering

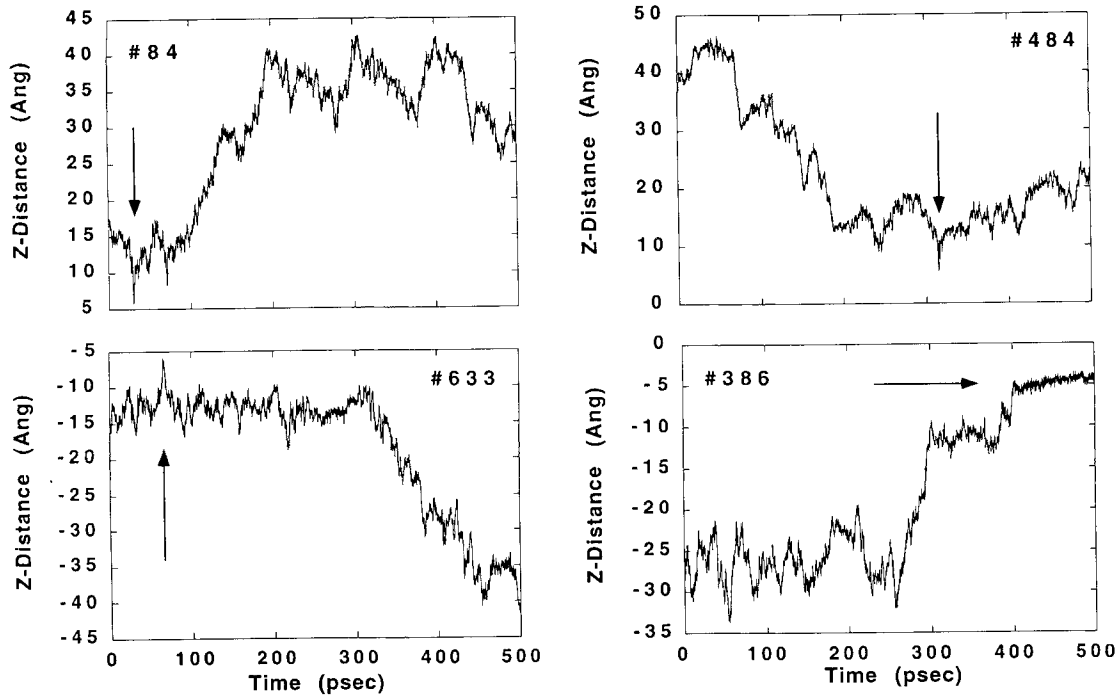

Fig. 10. Transient penetration by water molecules into the lipid bilayer. In three cases, the water entered and then exited again within 5 psec. In a fourth case, near the end of the 600 psec run, a water formed a stable hydrogen bond near the monomer–monomer junction.

the hydrocarbon region. On a speculative note, it is conceivable that such water molecules, attached to the outer surface of the channel, decrease the activation energy needed to break the monomer–monomer association and influence the stability of the dimer. For example, one of the six hydrogen bonds joining the monomers might be weakened by the formation of a transient hydrogen bond with a water outside the channel. The break in the monomer–monomer association is responsible for the abrupt interruptions in the ionic transmembrane current occurring on a time-scale of seconds that are observed during single channel recordings.[82]

Lipid–Protein Interactions

To characterize the lipid–protein interactions, the average distribution of interaction energies between individual lipids and protein was calculated. Figure 11 shows the interaction energy distribution function for individual lipid–GA interactions, averaged over all configurations (see the caption for details). The large peak centered around energies of a few kcal/mol corresponds to distant and weakly interacting DMPC:GA pairs. It arises because the interaction of the central channel with several of the distant lipid molecules located in the images is very weak. The interaction with lipid located in the images must also be included in the histogram because some of them can interact strongly with the central channel due to the spatial extend of the acyl chain. The smaller peak around −15 kcal/mol corresponds to the neighboring lipids in direct contact with the channel. A long tail, extending to −50 kcal/mol, is observed in the distribution, indicating that a small number of lipids interact very strongly with the channel. From the definition of the distribution function, the area under the curve in a given energy interval provides a direct estimate of the average number of lipid–gramicidin pairs interacting in that range of energy. For example, there are approximately 3 DMPC:GA pairs having an interaction energy between −20 and −50 kcal/mol, and there are around 10–13 DMPC:GA pairs having an interaction energy between −5 and −20 kcal/mol. The total number of DMPC:GA pairs between −5 and −50 is around 16, as expected from the number of DMPC surrounding the channel. The lower part of Figure 11 shows a breakdown of the lipid:GA interactions in terms of van der Waals and electrostatic contributions. It is clear that the relative contribution of each of these terms is nearly equal for those lipids strongly interacting with the GA. For those lipids interacting less strongly with the GA, the van der Waals term dominates, and there may even be a small unfavorable contribution from the electrostatic terms. Structurally this implies that there is both a strong van der Waals component from the hydrocarbon chains and a strong electrostatic com-

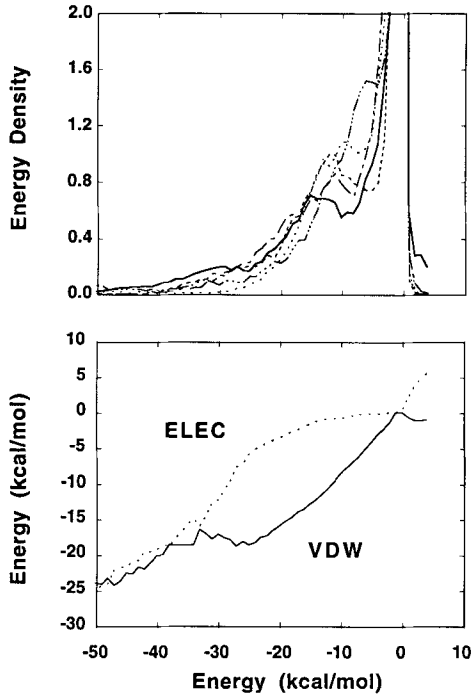

Fig. 11. Distribution of the interaction energies of individual lipid–GA pairs. The histogram shown in the top part was produced from the individual interaction energies. The individual interaction energies between the central channel and each of the lipid molecules (including the nearest images) were calculated from configurations saved every 0.5 psec and binned in 1.0 kcal/mol boxes. The count in each bin was divided by the bin width and the total number of configurations that were used so that the area under the curve in a given energy interval provides a direct estimate of the average number of lipid–gramicidin pairs interacting in that range of energy. The resulting profile shows the range of possible energetic interactions between lipid and protein. The larger energies reflect the possibility for favorable van der Waals and electrostatic interactions between both the headgroup and the hydrocarbon chains of the individual lipids. This is shown in the lower part, where the contribution from van der Waals and electrostatic terms for each bin is shown. Each of the lipids in the full trajectory was binned on the basis of its energetic interaction with the GA channel, and the relative probability of different energetic interactions determined.

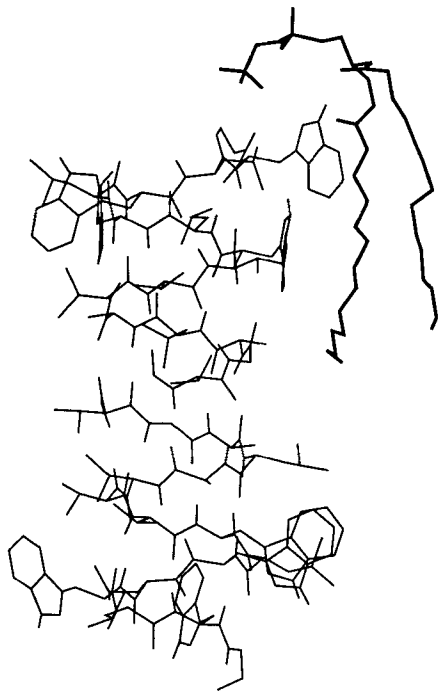

Fig. 12. A strongly interacting conformation between an individual lipid and GA. Note that one chain is in close van der Waals contact with the GA while the other chain is less strongly interacting with the GA.

ponent from the headgroup for the lipids interacting strongly with the channel.

Variations of the individual interactions between the DMPC lipids and the GA occur rapidly, showing that the strongly interacting lipids do not correspond to a single frozen conformation. The most strongly interacting conformations of lipid and protein are just as transient as the less strong conformations, lasting only tens of picoseconds. The lipid with the strongest interaction with GA is shown in Figure 12. Even though the van der Waals and electrostatic interactions are particularly strong for this lipid, the hydrocarbon chains do not form favorable van der Waals contacts with the GA over the full length of both chains. There is a hydrogen bond between the indole hydrogen of Trp-15 and the carbonyl oxygen of the ester group of the chain that is not in close van der Waals contact with GA. The headgroup conformation is such as to also increase the electrostatic and van der Waals connections between the headgroup and GA. One lipid chain is in close contact along much, but not all of the GA dimer. In particular, there is a close van der Waals contact between Trp-9 and the hydrocarbon chain of the lipid. It is possible to imagine even stronger transient interactions between the DMPC and the GA, even though such configurations were not observed here. Ordered configurations should be of low probability since the conformations of the hydrocarbon chains may be entropically disfavored. A wide range in energies is accessible for the protein–lipid interactions because the total interaction energy represents the sum of many weak interactions energies and does not represent a single energy well.

Lipid–Side Chain Interactions

The β-helical dimer conformation adopted by the GA channel in the phospholipid bilayer is such that the side chains extend directly into the membrane while the pore is formed by the backbone atoms.[12,48,83] Most of the side chains are hydrophobic and interact with the hydrocarbon chains. The residues near the membrane–solution interface, Trp-9, Trp-11, Trp-13, and Trp-15, and Leu-10, Leu-12, and Leu-14 are of particular interest since they can in-

teract with different components of the bilayer system. Their position suggests that they may be very important for mediating interactions between the protein and the environment. This can be seen in Figure 7 where the average density of the N-H atoms of Trp-9, Trp-11, Trp-13, and Trp-15 was shown in comparison with the average density of atoms in the immediate environment. The interactions of the tryptophans with the bilayer environment are an important factor in the stability of the β-helical structure of the GA dimer. Functional studies have demonstrated that they have an important influence on the conductivity and on the stability of the dimer channel.[84] Tests simulations of the channel in vacuum showed that large tryptophan fluctuations precede the destabilization and unfolding of the channel in 100–200 psec (data not shown). More generally, the presence of aromatic residues such as tryptophan, tyrosine, and phenylalanine near the membrane–solution interface is a structural feature that is often observed in membrane proteins (see above).[1,3,8,9,10,11,13,14]

To characterize the importance of the side chains, the average distribution of interaction energies between individual side chains and the membrane system was examined. For each configuration of the system, the total interaction energies of a particular side chain with the surrounding lipids and water was calculated and a histogram was constructed. The resulting averaged distribution of energy for interactions between individual tryptophans and both water and lipid is shown on the top part of Figure 13. The average of individual contributions corresponding to a given total lipid-side chain interaction energy is shown in the lower part. The interaction energy is decomposed in terms of the water, the hydrocarbon chains, the glycerol region, and the headgroup contributions. The energy density of the tryptophan residues is nearly gaussian, with a central peak around −19 kcal/mol. No significant variations were observed from one tryptophan residue to another in the character of the energy density and the results were combined for better statistical convergence. The breakdown of the contributions to the energy density shows that there is a nearly equal contribution from all four components for the most strongly interacting tryptophans. For the tryptophans interacting with energies less strong than −15 kcal/mol, the hydrocarbon chain component is the strongest, with the water and glycerol region coming next and the headgroup interaction being the smallest interaction. At the peak of the energy density, the hydrocarbon chain contribution is the largest, with the water, glycerol, and headgroup interactions being nearly the same. This shows that all four tryptophans can have significant interactions with both the bulk water and the different regions of the DMPC lipid molecules. In contrast, Figure 14 shows that the interaction between the leucine residues and the rest of

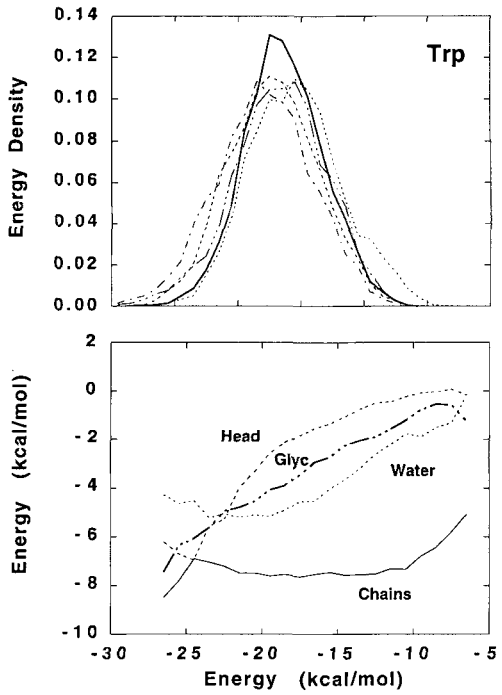

Fig. 13. Energetics of the interaction between tryptophans and their surroundings. The energetics of tryptophan interactions with lipid and water were analyzed in terms of the probability of a particular energy occurring. (**Top**) The probability density of particular total energetic interactions between individual tryptophan and both lipid and water is shown. The distribution function was normalized to unity.(**Bottom**) The breakdown of each energy term in terms of the lipid headgroup, the lipid glycerol group, the hydrocarbon chains, and the water is shown.

the system is dominated by van der Waals interactions with the hydrocarbon chains. There is a smaller contribution from the glycerol and headgroup regions of the lipids. The energy density distribution is also unimodal, indicating that the interactions of leucine residues with the surrounding are consistent with a single average environment. It is interesting to note that there is a nonzero interaction with the water molecules despite the hydrophobic character of the leucine side chains.

The time scale of the interactions between side chain and the rest of the system provides further information about the nature of lipid–protein interactions. The analysis shows that variations in the total energy of interaction are smaller than those of the individual components. For example, in the case of Trp-11 of monomer 1, the resulting total energy remains relatively constant, although considerable variations in the energies of interaction with the headgroup and the glycerol regions are observed. In another situation, Trp-9 of monomer 2, a near doubling of the total interaction energy occurred with concerted increases in the interactions of both the water and the glycerol regions. A similar analysis

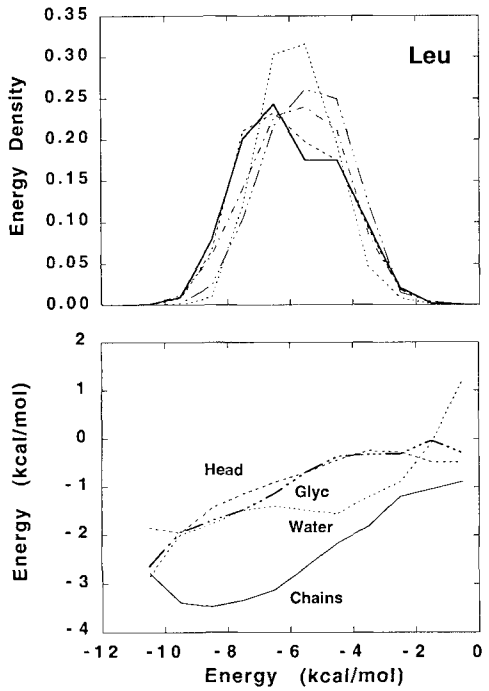

Fig. 14. Energetics of the interactions between leucine residues and their surroundings. The analysis is similar to Figure 13.

was made for the leucine side chains and their interactions with the lipid and water environment. The fluctuations in energy are less extreme, with, for example, the Leu-12 of side 2 varying between −4 and −8 kcal/mol over 500 psec. The largest change in this case is in the interaction of the leucine with the water and with the headgroup. In the case of the Leu-14 of monomer 1, concerted changes on the order of 2 kcal/mol in the interaction with water and the headgroups resulted in a nearly constant total energy of −7 kcal/mol. The total interaction energy for this particular leucine residue is nearly constant. However, the individual interactions of leucine with the various components (water, headgroups, etc.) fluctuate over time within a much broader range than the total energy.

The ability of the tryptophan indole ring to form hydrogen bonds is an important component of the interaction energies described above. An analysis was made of the type of hydrogen bonds formed by the indole hydrogen for each tryptophan within all five systems. The results of this analysis are shown in Table III. In particular, the table presents a breakdown of indole hydrogen bonding to water, glycerol, phosphate, and ethanolamine oxygens. The total time spent in hydrogen bonding for all tryptophans averaged near 50%. But, there are significant variations between the different simulations and between the two monomers within a given simulation. For all five systems, hydrogen bonding with water was the most prevalent. This was followed by (in order) the carbonyl ester oxygen, the ester oxygen, and the phosphoryl and the ester oxygens of the phosphate group. A short-lived hydrogen bond was also observed between Trp-9 and the oxygen of the ethanolamine moiety. The table shows some interesting variations between systems and between the different tryptophans. For example, the longest lived hydrogen bonding pattern for all five systems was for Trp-9 (third simulation), which spent 70% in hydrogen bonding with the ester carbonyl oxygens. There are large variations, however, for example, no hydrogen bond with the ester carbonyl oxygen was observed for Trp-9 in 2 monomers during 2 of the 5 simulations. Similarly for the water hydrogen bonding with Trp-9 the percent time varied from 53.5 to 1.3% for the second monomer of two different systems. Table III shows that Trp-15 had the longest time spent hydrogen bonding with the ester carbonyl oxygens. This is consistent with their significant overlap in the density profile shown in Figure 7. Surprisingly, Table III shows that Trp-9 and Trp-11 have a higher propensity to hydrogen bond than Trp-13. It is also interesting to note that there was a small incidence of hydrogen bonding between the ethanolamine tail and Trp-9 but not other tryptophans and also a small amount of hydrogen bonding between the phosphate group and Trp-15. This shows the degree of variability between the hydrogen bonding patterns observed on the hundreds of picosecond time scale between different systems. Two types of hydrogen bond involving the indole ring of the tryptophan side chain are illustrated on Figure 15. In one case (A), Trp-15 is making a hydrogen bond with the glycerol carbonyl group of the chain 2 of a DMPC molecule. In a second case (B), a bonding network involving Trp-9, two water molecules, and the phosphate group is shown. The packing of the hydrocarbon chains resulting from a Trp-DMPC hydrogen bond can also be observed in Figure 2 (see the lipid in the upper-right corner of the channel).

Figure 16 illustrates how different types of hydrogen bonds involving the indole N-H vary as a function of time. In general, a hydrogen bond with water was about five times shorter in duration and resulted in a smaller interaction energy than one with the carbonyl oxygen of the ester group of the lipid. This was despite the fact that the hydrogen bonds to water were more common than hydrogen bonds to lipid (see Table III). Figure 16 shows examples of hydrogen bonds with each of the tryptophans of the GA system. Part A of the Figure shows the interchange between water and carbonyl oxygen for Trp-13. Two different water hydrogen bonds are formed in the first 200 psec. A much longer lasting interaction with the carbonyl oxygens of one particular lipid is shown in the last two rows of Part A. Part B illustrates a particularly long lasting interaction between the carbonyl

TABLE III. Percent Hydrogen Bonding Occupancy of Trp*

Residue	Total	Water O	Gly C=O	Gly O	PC P=O	PC P—O	Eth O
Trp-9	43.8 19.7	33.9 14.3	9.7 0.2	0.2 0.8	0.0 0.0	0.0 4.4	0.0 0.0
	19.0 54.5	18.4 53.5	0.6 0.0	0.0 0.0	0.0 0.0	0.0 0.0	0.0 1.0
	34.6 72.5	29.4 1.3	5.2 70.2	0.0 1.0	0.0 0.0	0.0 0.0	0.0 0.0
	46.3 17.3	4.7 16.3	32.9 0.2	3.1 0.0	0.0 0.0	0.0 0.0	5.6 0.8
	46.5 32.4	46.1 32.4	0.0 0.0	0.0 0.0	0.0 0.0	0.0 0.0	0.4 0.0
	46.5 32.4	46.1 32.4	0.0 0.0	0.0 0.0	0.0 0.0	0.0 0.0	0.4 0.0
Average	38.7	25.0	11.9	0.5	0.0	0.4	0.8
Trp-11	49.6 58.8	4.9 58.5	44.7 0.3	0.0 0.0	0.0 0.0	0.0 0.0	0.0 0.0
	45.7 50.2	45.7 34.3	0.0 15.9	0.0 0.0	0.0 0.0	0.0 0.0	0.0 0.0
	43.9 58.5	43.3 20.8	0.6 37.3	0.0 0.4	0.0 0.0	0.0 0.0	0.0 0.0
	54.1 47.5	54.1 30.9	0.0 16.7	0.0 0.0	0.0 0.0	0.0 0.0	0.0 0.0
	46.5 40.6	41.8 39.2	0.0 0.0	0.0 1.4	1.8 0.0	2.9 0.0	0.0 0.0
Average	49.6	37.4	11.6	0.2	0.2	0.3	0.0
Trp-13	55.2 60.5	53.2 60.2	2.0 0.2	0.0 0.0	0.0 0.1	0.0 0.0	0.0 0.0
	53.1 25.5	52.9 19.4	0.2 5.1	0.0 1.0	0.0 0.0	0.0 0.0	0.0 0.0
	47.9 67.5	24.6 65.8	23.3 1.7	0.0 0.0	0.0 0.0	0.0 0.0	0.0 0.0
	49.2 52.7	34.8 51.2	14.4 0.0	0.0 0.0	0.0 1.2	0.0 0.2	0.0 0.0
	65.7 44.3	33.7 41.8	32.0 1.8	0.0 0.6	0.0 0.0	0.0 0.0	0.0 0.0
Average	52.2	43.8	8.1	0.2	0.1	0.0	0.0
Trp-15	39.9 57.0	28.5 10.0	0.0 47.0	0.1 0.0	1.6 0.0	9.7 0.0	0.0 0.0
	45.5 58.0	43.3 49.2	0.0 0.0	0.0 0.0	1.6 8.6	0.6 0.2	0.0 0.0
	56.9 50.4	37.5 15.4	15.2 26.2	0.0 0.0	0.4 6.3	3.8 2.5	0.0 0.0
	50.6 66.3	14.6 37.7	35.8 27.8	0.2 0.0	0.0 0.8	0.0 0.0	0.0 0.0
	62.2 54.5	28.0 30.2	0.2 1.6	0.0 0.0	26.1 0.2	8.0 22.4	0.0 0.0
Average	54.1	29.4	15.4	0.0	4.6	4.7	0.0

*Note that the 2 columns show the individual monomers for the GA. The first line is from the 600 psec trajectory, the other four lines are from the 300 psec trajectories. The average reflects both monomers and all five trajectories; the hydrogen bonds for this table were defined as indole N–H and oxygen within 2.3 Å of one another.

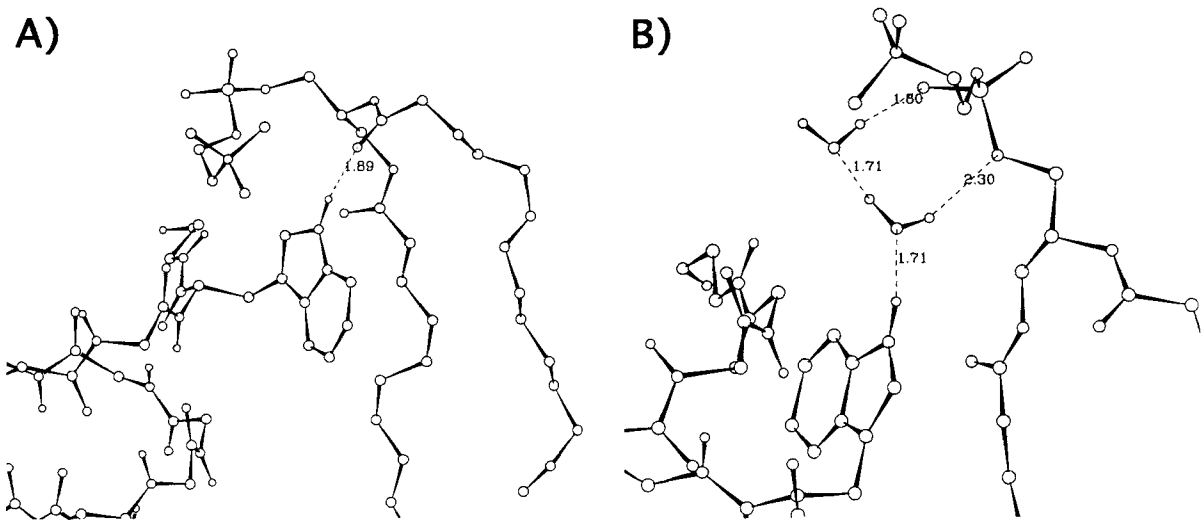

Fig. 15. Examples of hydrogen bonds formed by the tryptophan indole ring during the simulations. (**A**) Hydrogen bond of Trp-15 with a glycerol carbonyl group of the lipid. (**B**) Hydrogen bonding network involving Trp-9, two water molecules, and the polar headgroup.

oxygen of one lipid and the indole N–H of Trp-15. In this particular case, the hydrogen bond continued throughout most of the simulation. Part C shows three different water interactions with Trp-11, again emphasizing that they are briefer than the carbonyl oxygen interactions. Part D of the figure shows an example of exchange of lipid carbonyl ester oxygens from one lipid in the first part of the simulation to another lipid in the later part of the trajectory. Based on energy minimization, Wang and Pullman[43] sug-

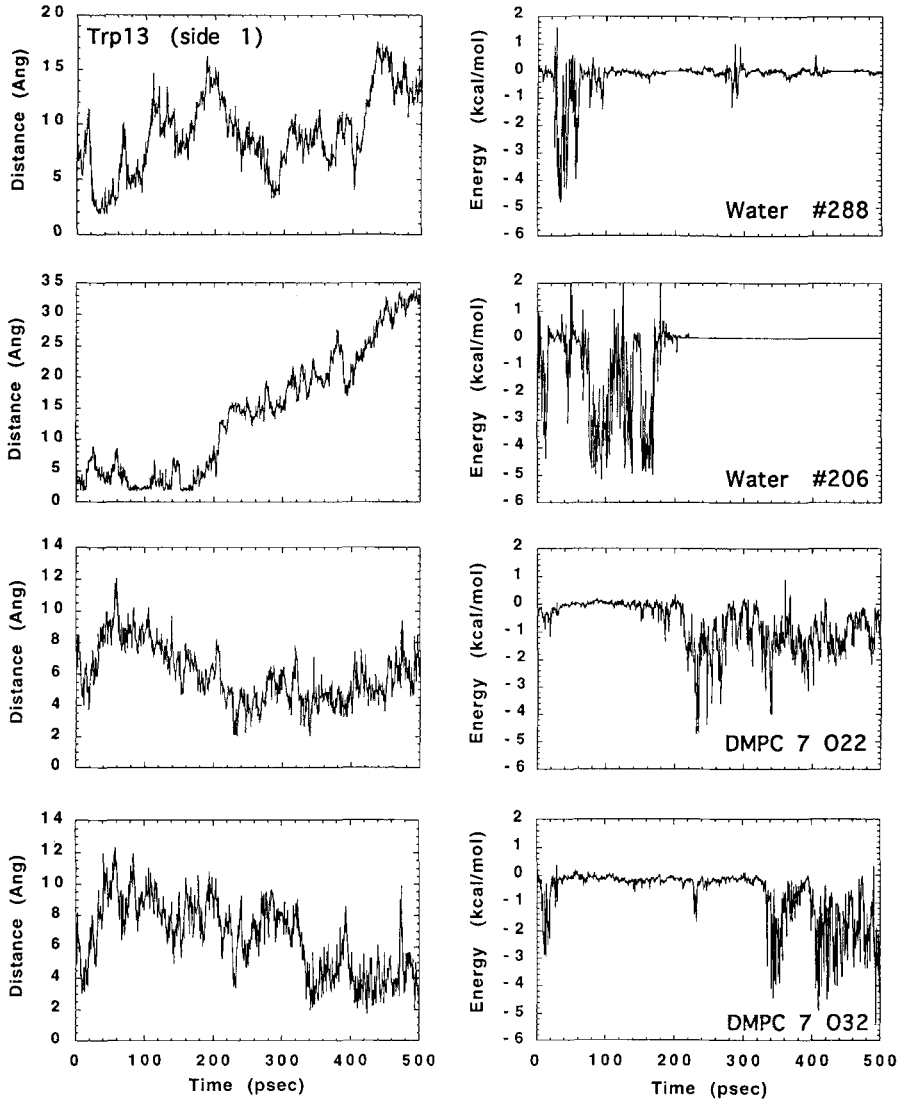

Fig. 16. Dynamics of hydrogen bonding between tryptophan and either water or lipid. The left-hand column shows the distance between the hydrogen bonding atoms, while the right-hand column shows the energies involved. In general, the water hydrogen bonds had a lifetime five times shorter than the bonds to the carbonyl ester oxygens of the DMPC lipids. (Figure continues on overleaf.)

gested that similar hydrogen bonding could occur in bilayers between the glycerol moiety of GMO and the N-H of the tryptophan indole ring. The present results, based on a dynamic trajectory, indicates that tryptophan–lipid hydrogen bonds can form but are transient in character. These observations are consistent with hydrogen exchange,[57] IR and Raman spectroscopy,[58] and fluorescence spectroscopy experiments,[85] which indicate that the tryptophans are motionally restricted due to presence of hydrogen bonds between the indole ring and the neighboring waters or the lipid carbonyls.

Comparison With Other Theoretical Models

A number of statistical mechanical models, such as the boundary lipid model of McConnell,[44] the mattress model of Mouritsen and Bloom,[45] and the lattice models of Zuckermann and Pink[46,47] have been proposed to address the thermodynamics of lipid–protein interactions. Despite the difficulty in relating such models with detailed atomic molecular dynamics simulations, it is useful to examine some of their central assumptions in light of the present results. The boundary lipid model is based on the assumption that the lipid molecules in direct contact with an intrinsic protein have significantly less conformational freedom that the free lipids.[44] The model has been generally used as a paradigm for thinking about lipid–protein interactions and to interpret the experimental results from ESR and NMR. In particular, the dependence of the DQS order parameters of DMPC on the GA concentration

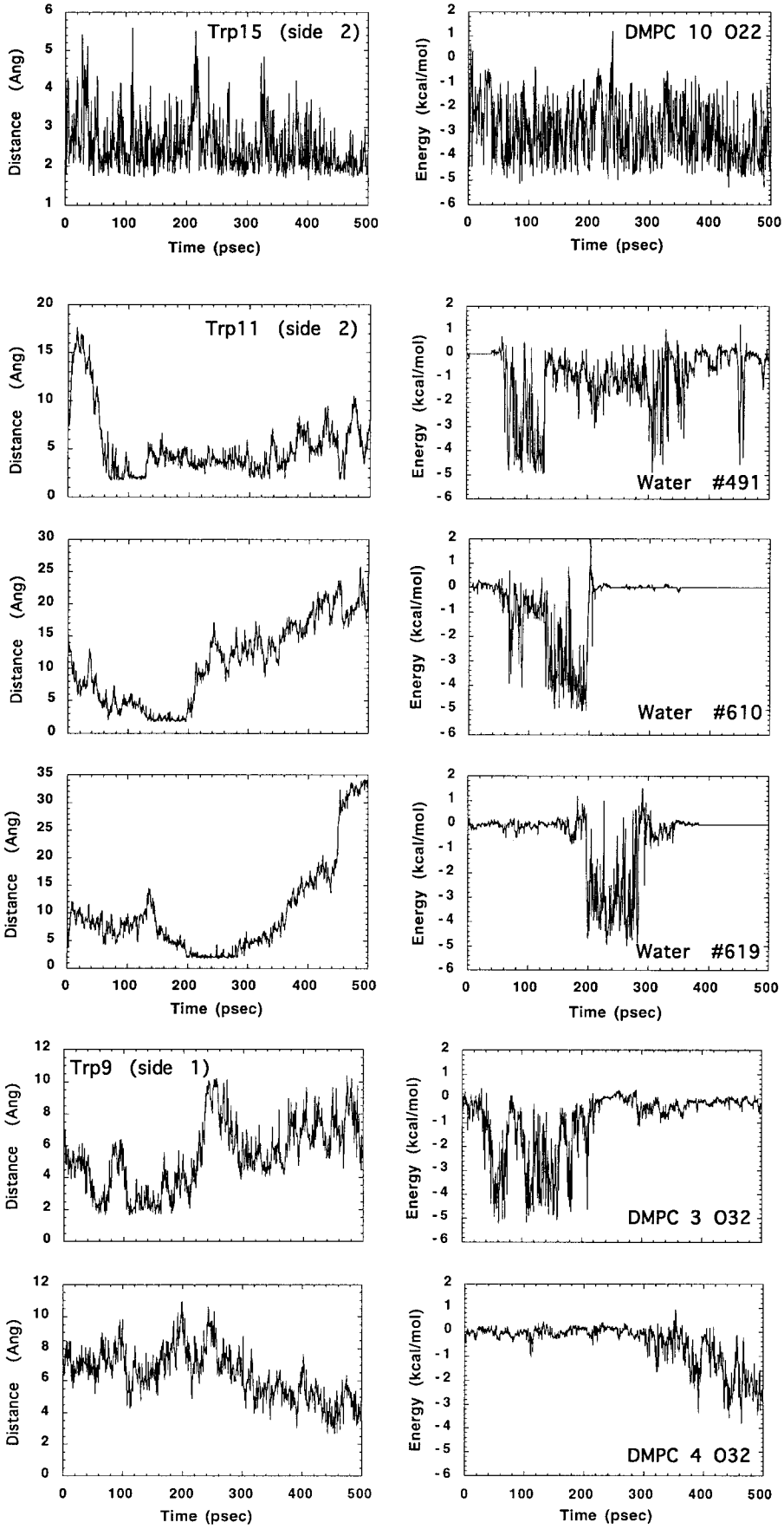

Fig. 16 (Continued)

was interpreted by Oldfield in the spirit of boundary lipids;[38] Yeagle and Kelsey, in a ^{31}P NMR study of glycophorin:phospholipid interactions, suggested the presence of a motionally restricted set of lipids near the protein.[86] The mattress model is based on the assumption that the dominant lipid–protein interaction involves the mismatch of the lengths of the hydrophobic regions of the phospholipid and the protein.[45,87] By relating the change in membrane thickness to the acyl chain order parameters, the mattress model could be used to interpret the influence of proteins on the DQS observed by solid-state NMR.[45] For example, the model correctly predicts the increase or decrease in acyl chain order induced by proteins whose hydrophobic length is longer or shorter than the equilibrium thickness of the host bilayer.[45,87,88] The models of Pink and Zuckermann[46] represent the membrane system as a two-dimensional lattice in which the lipid–protein interactions are described on the basis of discrete microstates related to the configuration of the hydrocarbon chains. Monte Carlo numerical simulations of these models provide information on the lateral organization of lipid bilayers systems and can be used to interpret data from calorimetry, in order to understand the phase behavior in such bilayer systems. Such lattice models have been extended to include lipid–cholesterol interactions, lipid–protein interactions, and the effect of foreign molecules (drugs, anesthetics, insecticides) on the physical properties of lipid bilayer systems.[47]

Although those models have been helpful in interpreting the data from experiments, the present study indicates that some important aspect of the interactions of proteins with phospholipid bilayers are not taken into account. In particular, very rapid variations of the interaction energy between one DMPC molecule and the GA were observed in the present simulations. In contrast with the boundary lipid model,[44] the most strongly interacting conformations do not correspond to a single long-lived, frozen lipid conformer. Those conformations, such as that represented in Figure 12, fluctuate rapidly on a time-scale of tens of picoseconds. The very wide range of lipid–protein interactions observed here should be considered in describing the boundary lipids. In adition, even though a slight thickening of the bilayer was observed in the present simulations, it appears to be a consequence of the ordering of the lipid chains in direct contact with the surface of the GA rather than a result of a mismatch between the hydrocarbon region of the bilayer and the length of the channel as described by the mattress model.[45,87] In fact, the thickness of the hydrocarbon chain region for a DMPC bilayer should be well-matched to the 23 Å long GA channel.[25] An important assumption of the mismatch model is that the boundary of the hydrophobic part of the protein and the membrane is well-defined. In contrast, the width of the interfacial region is on the order of 12–14 Å on each side of the bilayer, and the total thickness of the hydrophobic region is on the order of 24 Å (see Fig. 7). Furthermore, the influence of interactions of the protein with the glycerol and the polar head regions of the lipid can be important. Some components of those interactions are polar and involved hydrogen bonding of amphipathic side chains. Lastly, the configurations in the lipid:protein system are characterized by significant deviations from two-dimensional lattice symmetry (see Fig. 2). The accessible states are not determined simply by the available cross-sectional area of a lipid conformer, as assumed in the lattice models,[46,47] but are also influenced by detailed packing interactions.[41,42]

The statistical mechanical models could be made more realistic by taking some of the main features observed in the current simulations into account. For example, the significant width of the membrane–solution interface could be incorporated in the mismatch between the hydrophobic surfaces of the protein and the hydrocarbon core of the membrane; the large spread in the distribution of the interaction energies between the protein and individual lipids could be included in the mattress model. Nevertheless, an exact correspondence is difficult to make because the simplified models are constructed with effective interaction parameters representing free energy of interactions rather than true microscopic interactions.

CONCLUSION

The microscopic details of lipid–protein interactions were examined using molecular dynamics simulations of the GA channel embedded in a fully hydrated DMPC bilayer. A novel method was used to assemble the initial configurations of the atomic systems from preequilibrated and prehydrated phospholipid molecules. Three sets of 100 systems, corresponding to three choices of cross-sectional area for the GA and the DMPC, were constructed with different initial lipid configurations. Seven systems were simulated with molecular dynamics. One system was simulated for a total of 600 psec, four were simulated for 300 psec, and two for 100 psec. The present construction approach is general and can be used to generate starting configuration for membrane proteins of any shape in a bilayer environment.

The simulations were analyzed in terms of average structure, energetics, and dynamics. Throughout the trajectories, the structure of the protein–membrane complex remained stable. Analysis of the configurational evolution of the DMPC molecules indicates that the simulation systems were equilibrated after 100 psec. Thus, the construction method appears to have shortened significantly the simulation time needed to equilibrate the system, and offers significant improvements over starting from an

all-*trans* state or manually model building lipids around a membrane protein. The average density profile of the main components of the system, shown in Figure 7, reveals that the membrane–solution interface region is much broader than pictured traditionally. Usage of the word interface is almost inappropriate in the present case since the thickness of the transition region is comparable to that of the full hydrophobic region. The DQS of the lipid acyl chains, calculated from both a time and an *ensemble* average on the basis of five trajectories, are in good agreement with the available experimental data. An important result is that there is an ordering of the lipid chains in direct contact with the GA, but the effect is not uniform due to the irregular surface of the protein.

The range of interaction energies for the lipids and the protein is also very broad. The interactions of the channel with the neighboring lipids are around −15 kcal/mol on average, although they can extend to −50 kcal/mol for some configurations. Individual lipid–protein interactions fluctuate over a wide range on a time scale of 50–500 psec. The most strongly interacting configurations are transient in nature and do not involve a single frozen conformation throughout the full simulation. The total interactions results from a sum over a large number of small individual van der Waals and electrostatic contributions. The interaction energy between individual amino acids and lipid or water is relatively constant, although analysis of particular cases shows that the total interaction resulted from many contributions fluctuating over a wide range. For example, the average −8 kcal/mol interaction energy for the leucine with lipid and water is maintained nearly constant, despite fluctuations from −5 kcal/mol to 0 in the individual leucine–water, leucine–glycol, leucine–headgroup, and leucine–hydrocarbon chain interactions. The tryptophans, located at the transition between the hydrophobic core of the membrane and the bulk solution, appear to be particularly important in mediating both hydrogen bonding interactions with the lipid glycerol backbone and water and also in forming favorable van der Waals contacts with the lipid hydrocarbon chains. In contrast, the interactions of the leucine residues with the lipids, also located near the interface, are dominated by van der Waals interactions with the lipid hydrocarbon chains.

The complex composition of the broad transition extending from the hydrophobic core of the membrane to the bulk water region appears to particularly favorable for residues such as the tryptophans. This may be an important factor in the folding and in the stability of secondary and tertiary structural elements of membrane proteins. Traditionally, empirical scales based on the thermodynamics of transfer from a hydrophobic to a hydrophilic environment have been used to estimate the likelihood of particular residues to be located in solution or inside the bilayer.[4–7] More realistically, the structure of the bilayer is that of a 24-Å-thick hydrophobic hydrocarbon chain region surrounded by a 12- to 14-Å-thick transitions, extending from the membrane core to the bulk water. The transition is composed of the glycerol lipid backbone, the polar headgroup, and strongly bound waters. Such representation could be used to improve current structure prediction algorithms. Additional insight into the factors involved in the folding and stability of membrane proteins and membrane peptides might be gained from thermodynhamic experiments examining the partition coefficient of amino acids in a 1:1:1 solution mixture of water:glycerol:phosphocholine relative to water and hydrocarbon solutions. Structural studies on small membrane-bound peptides could provide more information on the interaction of particular residue at the interface.

The insight generated by the present molecular dynamics simulations begins to provide a sound basis for viewing protein–lipid interactions at the molecular level. This suggests that molecular dynamics simulations will be a powerful tool in exploring the microscopic details of lipid–protein interactions. Further work is currently in progress on other membrane protein systems.

ACKNOWLEDGMENTS

The financial support of MRC is gratefully acknowledged.

REFERENCES

1. Deisenhofer, J., Michel, H. The photosynthetic reaction center from the purple bacterium rhodopseudomonas viridis. Science 245:1463–1473, 1989.
2. Henderson, R., Baldwin, J.M., Ceska, T.A., Zemlin, F., Beckmann, E., Downing, K.H. Model for the structure of bacteriorhodopsin based on high-resolution electron cryomicroscopy. J. Mol. Biol. 213:899–929, 1990.
3. Shon, K., Kim, Y., Colnago, L.A., Opella, S.J. Nmr studies of the structure and dynamics of membrane-bound bacteriophage pf1 coat protein. Science 252:1303–1305, 1991.
4. Eisenberg, D., Weiss, R.M., Terwilliger, T.C. The helical hydrophobic moment: A measure of the amphiphilicity of a helix. Nature (London) 299:371–374, 1982.
5. Engelman, D.M., Steitz, T.A., Goldman, A. Identifying nonpolar transbilayer helices in amino acid sequences of membrane proteins. Annu. Rev. Biophys. Biophys. Chem. 15:321–353, 1986.
6. Wesson, L., Eisenberg, D. Atomic solvation parameters applied to molecular dynamics of proteins in solution. Protein Sci. 1:227–235, 1992.
7. Edholm, O., Jahnig, F. The structure of a membrane-spanning polypeptide studied by molecular dynamics. Biophys. Chem. 30:279–292, 1988.
8. Cowan, S.W., Schirmer, T., Rummel, G., Steiert, M., Gosh, R., Pauptit, R.A., Jansonius, J.N. Crystal structures explain functional properties of two E. coli porins. Nature (London) 358:727–733, 1992.
9. Weiss, M.S., Schulz, G.E. Structure of porin refined at 1.8 Å resolution. J. Mol. Biol. 227:493–509, 1992.
10. McDonnell, P.A., Shon, K., Kim, Y., Opella, S.J. fd coat protein structure in membrane environments. J. Mol. Biol. 233:447–463, 1993.
11. Picot, D., Loll, P.J., Garavito, R.M. The X-ray structure of the membrane protein prostaglandin H_2 synthase-1. Nature (London) 367:243–249, 1994.

12. Ketchem, R.R., Hu, W., Cross, T.A. High-resolution conformation of gramicidin A in lipid bilayer by solid-state nmr. Science 261:1457–1460, 1993.
13. White, J. Membrane fusion. Nature (London) 258:917–924, 1992.
14. Landolt-Marticorena, C., Williams, K.A., Deber, C.M., Reithmeier, R.A.F. Nonrandom distribution of amino acids in the transmembrane segments of human type i single span membrane proteins. J. Mol. Biol. 229:602–608, 1993.
15. Jacobs, R.E., White, S.H. The nature of the hydrophobic binding of small peptides at the bilayer interface: Implications for the insertion of transbilayer helices. Biochemistry 28:3421–3437, 1989.
16. Brooks, C.L., III, Karplus, M., Pettitt, B.M. Proteins. A theoretical perspective of dynamics, structure and thermodynamics. In: "Advances in Chemical Physics," Vol. LXXI. Prigogine, I., Rice, S.A. (eds.). New York: John Wiley, 1988.
17. Pastor, R.W. Molecular dynamics and Monte Carlo simulations of lipid bilayers. Curr. Opin. Struc. Biol. 4:486–492, 1994.
18. Egberts, E. Molecular dynamics simulation of multibilayer membranes. Ph.D. Thesis, Univ. Groningen, 1988.
19. Loof, H.D., Harvey, S.C., Segrest, J.P., Pastor, R.W. Mean field stochastic boundary molecular dynamics simulation of a phospholipid in a membrane. Biochemistry 30:2099–2113, 1991.
20. Bassolino-Klimas, D., Alper, H.E., Stouch, T.R. Solute diffusion in lipid bilayer membranes: An atomic level study by molecular dynamics simulation. Biochemistry 32: 12624–12637, 1993.
21. Merz, K.M., Damodaran, K.V. A comparison of DMPC- and DLPE-based lipid bilayers. Biophys J. 66:1076–1087, 1994.
22. Venable, R.M., Zhang, Y., Hardy, B.J., Pastor, R.W. Molecular dynamics simulations of a lipid bilayer and of hexadecane: An investigation of membrane fluidity. Science 262:223–226, 1993.
23. Pascher, I., Lundmark, M., Nyholm, P.G., Sundell, S. Crystal structures of membrane lipids. Biochim. Biophys. Acta 1113:339–373, 1992.
24. Hauser, H., Pascher, I., Pearson, R.H., Sundell, S. Preferred conformation and molecular packing of phosphatidylethanolamine and phosphatidylcholine. Biochim. Biophys. Acta 650:21–51, 1981.
25. Engelman, D.M., Lewis, B.A. Lipid bilayer thickness varies linearly with acyl chain length in fluid phosphatidylcholine vesicles. J. Mol. Biol. 166:211–217, 1983.
26. Ulrich, A.S., Volke, F., Watts, A. The dependence of phospholipid head-group mobility on hydration as studied by deuterium-nmr spin-lattice relaxation time measurements. Chem. Phys. Lipids 55:61–66, 1990.
27. Bechinger, B., Seelig, J. Conformational changes of the phosphatidylcholine headgroup due to membrane dehydration. A ^{2}H-nmr study. Chem. Phys. Lipids 58:1–5, 1991.
28. Woolf, T.B., Roux, B. Molecular dynamics simulations of proteins in lipid membranes: The first steps. Biophys. J. A354:1993.
29. Woolf, T.B., Roux, B. Molecular dynamics simulations of lipid:protein interactions: Gramicidin A in a dmpc bilayer. Biophys. J. A348:1994.
30. Woolf, T.B., Desharnais, J., Roux, B. Structure and dynamics of the sidechains of gramicidin in a DMPC bilayer. In "NATO ASI Series: Computational Approaches in Supramolecular Chemistry," Vol. 426. Wipff, G. (ed.). Dordrecht: Kluwer Academic Publishers, 1994:519–531.
31. Woolf, T.B., Roux, B. Molecular dynamics simulation of the gramicidin channel in a phospholipid bilayer. Proc. Natl. Acad. Sci. U.S.A. 91:11631–11635, 1994.
32. Pastor, R.W., Venable, R.M., Karplus, M. Model for the structure of the lipid bilayer. Proc. Natl. Acad. Sci. U.S.A. 88:892–896, 1991.
33. Smith, R., Thomas, D.E., Separovic, F., Atkins, A.R., Cornell, B.R. Determination of the structure of a membrane-incorporated ion channel. Biophys. J. 56:307–314, 1989.
34. Prosser, R.W., Davis, J.H., Dahlquist, F.W., Lindorfer, M.A. 2h nuclear magnetic resonance of the gramicidin A backbone in a phospholipid bilayer. Biochemistry 30: 4687–4696, 1991.
35. Andersen, O.S., Koeppe, R.E., II. Molecular determinants of channel function. Physiol. Rev. 72:S89–S158, 1992.
36. Killian, J.A. Gramicidin and gramicidin-lipid interactions. Biochim. Biophys. Acta 1113:391–425, 1992.
37. Roux, B., Karplus, M. Molecular dynamics simulations of the gramicidin channel. Annu. Rev. Biomol. Struc. Dyn. 23:731–761, 1994.
38. Rice, D., Oldfield, E. Deuterium nuclear magnetic resonance studies of the interaction between dimyristoylphosphatidylcholine and gramicidin A. Biochemistry 18:3272–3279, 1979.
39. Watnick, P.I., Chan, S.I., Dea, P. Hydrophobic mismatch in gramicidin A'/lecithin systems. Biochemistry 29:6215–6221, 1990.
40. Davies, J.A., Braunder, J.W., Schuster, H.F., Mendelsohn, R. A quantitative infrared determination of acyl chain conformation in gramicidin/dipalmitoylphosphatidylcholine mixtures. Biochem. Biophys. Res. Commun. 168:85–90, 1990.
41. Xing, J., Scott, H.L. Monte carlo studies of lipid chains and gramicidin a in a model membrane. Biochem. Biophys. Res. Commun. 165:1–6, 1989.
42. Xing, J., Scott, H.L. Monte carlo studies of a model for lipid-gramicidin A bilayers. Biocheim. Biophys. Acta 1106: 227–232, 1992.
43. Wang, J., Pullman, A. The intrinsic molecular potential of glyceryl monooleate layers and its effect on the conformation and orientation of an inserted molecule: Example of gramicidin A. Biochim. Biophys. Acta 1024:10–18, 1990.
44. Owicki, J.C., Springgate, M.W., McConnell, H.M. Theoretical study of protein-lipid interactions in bilayer membranes. Proc. Natl. Acad. Sci. U.S.A. 75:1616–1619, 1978.
45. Mouritsen, O.G., Bloom, M. Mattress model of lipid-protein interactions in membranes. Biophys. J. 46:141–153, 1984.
46. Zuckermann, M.J., Pink, D.A. The correlation length and lateral compressibility of phospholipid bilayers in the presence of thermodynamic density fluctuations. J. Chem. Phys. 73:2919–2926, 1980.
47. Zhang, Z., Sperotto, M.M., Zuckermann, M.J., Mouritsen, O.G. A microscopic model for lipid/protein bilayers with critical mixing. Biochim. Biophys. Acta 1147:154–160, 1993.
48. Arseniev, A.S., Bystrov, V.F., Ivanov, T.V., Ovchinnikov, Y.A. ^{1}H-NMR study of gramicidin-A transmembrane ion channel. Head-to-head right-handed, single stranded helices. FEBS 186:168–174, 1985.
49. Roux, B., Karplus, M. Ion transport in the gramicidin channel: Free energy profile along the right-handed dimer. J. Am. Chem. Soc. 115:3250–3260, 1993.
50. Mackerell, A.D., Jr., Bashford, D., Bellot, M., Dunbrack, R.L., Field, M.J., Fischer, S., Gao, J., Guo, H., Joseph, D., Ha, S., Kuchnir, L., Kuczera, K., Lau, F.T.K., Mattos, C., Michnick, S., Nguyen, D.T., Ngo, T., Prodhom, B., Roux, B., Schlenkrich, B., Smith, J., Stote, R., Straub, J., Wiorkiewicz-Kuczera, J., Karplus, M. Self-consistent parametrization of biomolecules for molecular modelling and condensed phase simulations. Biophys. J. 61:A143, 1992.
51. Jorgensen, W.L., Impey, R.W., Chandrasekhar, J., Madura, J.D., Klein, M.L. Comparison of simple potential functions for simulating liquid water. J. Chem. Phys. 79: 926–935, 1983.
52. Davis, J.H. Personal communication, 1993.
53. Gunsteren, W.F., Berendsen, H.J.C. Algorithms for macromolecular dynamics and constraint dynamics. Mol. Phys. 34:1311–1327, 1977.
54. Woolf, T.B., Roux, B. The conformation flexibility of o-phosphorylcholine and o-phosphorylethanolamine: A molecular dynamics study of solvation effects. J. Am. Chem. Soc. 116:5916–5926, 1994.
55. Pastor, R.W., Venable, R.M., Karplus, M. Brownian dynamics simulation of a lipid chain in a membrane bilayer. J. Chem. Phys. 89:1112–1127, 1988.
56. Hardy, B.J., Pastor, R.W. Conformation sampling of hydrocarbon and lipid chains in an orienting potential. J. Comput. Chem. 15:208–226, 1994.
57. Takeuchi, H., Nemoto, H., Harada, I. Environments and conformations of tryptophan side chains of gramicidin A in phospholipid bilayers studied by raman spectroscopy. Biochemistry 29:1572–1579, 1990.

58. Bouchard, M., Auger, M. Solvent history dependence of gramicidin-lipid interactions: A Raman and infrared spectroscopic study. Biophys. J. 65:2484–2492, 1993.
59. Brooks, B.R., Bruccoleri, R.E., Olafson, B.D., States, D.J., Swaminathan, S., Karplus, M. CHARMM: A program for macromolecular energy minimization and dynamics calculations. J. Comput. Chem. 4:187–217, 1983.
60. Heller, H., Schaefer, M., Schulten, K. Molecular dynamics simulation of a bilayer of 200 lipids in the gel and in the liquid-crystal phases. J. Phys. Chem. 97:8343–8360, 1993.
61. Pastor, R.W. Personal communication, 1993.
62. Pace, R.J., Chan, S.I. Molecular motions in lipid bilayers i. Statistical mechanical model of acyl chain motion. J. Chem. Phys. 76:4217–4227, 1982.
63. Nagle, J.F., Wiener, M.C. Structure of fully hydrated bilayer dispersions. Biochim. Biophys. Acta 942:1–10, 1988.
64. Schindler, H., Seelig, J. Deuterium order parameters in relation to thermodynamic properties of a phospholiped bilayer: A statistical mechanical interpretation. Biochemistry 14:2283–2287, 1975.
65. Nagle, J.F. Area/lipid of bilayers from nmr. Biophys. J. 64:1476–1481, 1993.
66. De Young, L.R., Dill, K.A. Solute partitioning into lipid bilayer membranes. Biochemistry 27:5281–5289, 1988.
67. Thurmond, R.L., Dodd, S.W., Brown, M.F. Molecular areas of phospholipids as determined by 2h nmr spectroscopy: Comparison of phosphatidylethanolamines and phosphatidylcholines. Biophys. J. 59:108–113, 1991.
68. Kemp, G., Jacobson, K.A., Wenner, C. Solution and interfacial properties of gramicidin pertinent to its effect on membranes. Biochim. Biophys. Acta 255:493–501, 1972.
69. Kemp, G., Wenner, C. Solution, interfacial, and membrane properties of gramicidin A. Arch. Biochem. Biophys. 176: 547–555, 1976.
70. Ries, H.E., Swift, H. Monolayers of two transmembrane channel formers and an ionophore. J. Colloid Interface Sci. 117:584–588, 1987.
71. Dhathathreyan, A., Baumann, U., Muller, A., Mobius, D. Characterization of complex gramicidin monolayers by light reflection and fourier transform infrared spectroscopy. Biochim. Biophys. Acta 944:265–272, 1988.
72. Mau, N.D.-V., Daumas, P., Lelievre, D., Trudelle, Y., Heitz, F. Linear gramicidins at the air-water interface. Biophys. J. 51:843–845, 1987.
73. Tournois, H., Gieles, P., Demel, R., de Gier, J., de Kruijff, B. Interfacial properties of gramicidin and gramicidin-lipid mixtures measured with static and dynamic monolayer techniques. Biophys. J. 55:557–569, 1989.
74. Buldt, G., Gally, H.U., Seelig, J., Zaccai, G. Neutron diffraction studies on phosphatidylcholine model membranes. I. head group conformation. J. Mol. Biol. 134:673–691, 1979.
75. Zaccai, G., Buldt, G., Seelig, A., Seelig, J. Neutron diffraction studies on phosphatidylcholine model membranes. II. chain conformation and segmental disorder. J. Mol. Biol. 134:693–706, 1979.
76. Seelig, J. 31P nuclear magnetic resonance and the head group structure of phospholipids in membranes. Biochim. Biophys. Acta 515:105–140, 1978.
77. Seelig, J., Macdonald, P.M., Scherer, P.G. Phospholipid head groups as sensors of electric charge in membranes. Biochemistry 26:7535–7541, 1987.
78. Moll, F., III, Cross, T.A. Optimizing and characterizing alignment of oriented lipid bilayers containing gramicidin D. Biophys. J. 57:351–362, 1990.
79. Pink, D.A., Georgallas, A., Chapman, D. Intrinsic proteins and their effect upon lipid hydrocarbon chain order. Biochemistry 20:7152–7157, 1981.
80. Seelig, J., Seelig, A. Lipid conformation in model membranes and biological membranes. Q. Rev. Biophys. 13:19–61, 1980.
81. Ho, C. Hydration at the membrane protein–lipid interface. Biophys. J. 63:897–902, 1992.
82. Hladky, S.B., and Haydon, D.A. Ion transfer across lipid membranes in the presence of gramicidin A. I. studies of the unit conductance channel. Biochim. Biophys. Acta 274: 294–312, 1972.
83. Urry, D.W. The gramicidin A transmembrane channel: A proposed pi(l,d) helix. Proc. Natl. Acad. Sci. U.S.A. 68:672–676, 1971.
84. Becker, M.D., Greathouse, D.V., Koeppe, R.E., II, Andersen, O.S. Amino acid sequence modulation of gramicidin channel function: Effects of tryptophane-to-phenylalanine substitutions on the single-channel conductance and duration. Biochemistry 30:8830–8839, 1991.
85. Mukherjee, S., Chattopadhyay, A. Motionall restricted tryptophan environments at the peptide–lipid interface of gramicidin channels. Biochem. 33:5089–5097, 1994.
86. Yeagle, P.L., Kelsey, D. Phosphorus nuclear magnetic resonance studies of lipid-protein interactions: Human erythrocyte glycophorin and phospholipids. Biochemistry 28: 2210–2215, 1989.
87. Mouritsen, O.G., Bloom, M. Models of lipid-protein interactions in membranes. Annu. Rev. Biophys. Biomol. Struct. 22:145–171, 1993.
88. Nezil, F.N., Bloom, M. Combined influence of cholesterol and synthetic amphiphillic peptides upon bilayer thickness in model membranes. Biophys. J. 61:1176–1183, 1992.
89. He, K., Ludtke, SJ., Wu, Y., Huang, H.W. X-ray scattering with momentum transfer in the plane of membrane. Application to gramicidin organization. Biophys. J. 64:157–162, 1993.